NAVAL POSTGRADUATE SCHOOL
Monterey, California

THESIS

EXAMINATION OF THE USE OF EXACT VERSUS APPROXIMATE PHASE WEIGHTS ON THE PERFORMANCE OF A SYNTHETIC APERTURE SONAR SYSTEM

by

Matthew R. Boland

March 2003

Thesis Advisor: Lawrence J. Ziomek
Second Reader: Xiaoping Yun

THIS PAGE INTENTIONALLY LEFT BLANK

REPORT DOCUMENTATION PAGE

Form Approved OMB No. 0704-0188

1. AGENCY USE ONLY *(Leave blank)*	2. REPORT DATE	3. REPORT TYPE AND DATES COVERED
	March 2003	Master's Thesis

4. TITLE AND SUBTITLE Examination of the Use of Exact Versus Approximate Phase Weights on the Performance of a Synthetic Aperture Sonar System

5. FUNDING NUMBERS

6. AUTHOR (S) Matthew R. Boland

7. PERFORMING ORGANIZATION NAME(S) AND ADDRESS(ES)
Naval Postgraduate School
Monterey, CA 93943-5000

8. PERFORMING ORGANIZATION REPORT NUMBER

9. SPONSORING / MONITORING AGENCY NAME(S) AND ADDRESS(ES)

10. SPONSORING/MONITORING AGENCY REPORT NUMBER

11. SUPPLEMENTARY NOTES The views expressed in this thesis are those of the author and do not reflect the official policy or position of the U.S. Department of Defense or the U.S. Government.

12a. DISTRIBUTION / AVAILABILITY STATEMENT
Approved for public release; distribution is unlimited

12b. DISTRIBUTION CODE

13. ABSTRACT ***(maximum 200 words)***

Synthetic aperture sonar beamforming and signal processing relies on properly steering and focusing the aperture beam pattern in order to co-phase all the received signals. Due to the effects of motion in the synthetic aperture sonar problem, the propagation path between the transmitter, discrete point scatterer, and the receiver is time varying. Traditionally, simple approximations are used to determine these propagation ranges and angles of incidence and scatter. Methods to determine these ranges and angles exactly may significantly improve array gain and, therefore, target detection.

This thesis investigates improvements to SAS signal processing algorithms using exact methods for the calculation of the time-varying ranges between transmitter and discrete point scatter, and between discrete point scatter and receiver, and the phase angle of the scattered acoustic signal incident upon the receiver. Using computer simulations, exact range and angle calculations were performed for different scenarios and compared to ranges and angles determined using standard approximations. The exact ranges were then used to determine incident phase, and were again compared to the approximate methods. Comparison of the exact and approximate methods was based on range estimation error and percentage error. Improvements in synthetic aperture array gain using exact phase weights based on exact, time-varying range solutions are proposed.

14. SUBJECT TERMS	15. NUMBER OF PAGES
Synthetic Aperture Sonar, SAS, Bistatic Scattering, UUV, Mine Warfare	83
	16. PRICE CODE

17. SECURITY CLASSIFICATION OF REPORT	18. SECURITY CLASSIFICATION OF THIS PAGE	19. SECURITY CLASSIFICATION OF ABSTRACT	20. LIMITATION OF ABSTRACT
Unclassified	Unclassified	Unclassified	UL

NSN 7540-01-280-5500 **Standard Form 298 (Rev. 2-89) Prescribed by ANSI Std. 239-18**

THIS PAGE INTENTIONALLY LEFT BLANK

Approved for public release; distribution is unlimited

EXAMINATION OF THE USE OF EXACT VERSUS APPROXIMATE PHASE WEIGHTS ON THE PERFORMANCE OF A SYNTHETIC APERTURE SONAR SYSTEM

Matthew R. Boland
Lieutenant, United States Navy
B.S., United States Naval Academy, 1996

Submitted in partial fulfillment of the
requirements for the degree of

MASTER OF SCIENCE IN ELECTRICAL ENGINEERING

from the

NAVAL POSTGRADUATE SCHOOL
March 2003

Author: Matthew R. Boland

Approved by: Lawrence J. Ziomek
Thesis Advisor

Xiaoping Yun
Second Reader

John Powers
Chairman, Electrical and Computer Engineering Department

THIS PAGE INTENTIONALLY LEFT BLANK

ABSTRACT

Synthetic aperture sonar beamforming and signal processing relies on properly steering and focusing the aperture beam pattern in order to co-phase all the received signals. Due to the effects of motion in the synthetic aperture sonar problem, the propagation path between the transmitter, discrete point scatterer, and the receiver is time varying. Traditionally, simple approximations are used to determine these propagation ranges and angles of incidence and scatter. Methods to determine these ranges and angles exactly may significantly improve array gain and, therefore, target detection.

This thesis investigates improvements to SAS signal processing algorithms using exact methods for the calculation of the time-varying ranges between transmitter and discrete point scatter, and between discrete point scatter and receiver, and the phase angle of the scattered acoustic signal incident upon the receiver. Using computer simulations, exact range and angle calculations were performed for different scenarios and compared to ranges and angles determined using standard approximations. The exact ranges were then used to determine incident phase, and were again compared to the approximate methods. Comparison of the exact and approximate methods was based on range estimation error and percentage error. Improvements in synthetic aperture array gain using exact phase weights based on exact, time-varying range solutions are proposed.

THIS PAGE INTENTIONALLY LEFT BLANK

TABLE OF CONTENTS

LIST OF FIGURES

ACKNOWLEDGEMENTS

I am indebted to the faculty of Electrical Engineering Department at the Naval Postgraduate School. Their commitment to excellence and passion for teaching was the highlight of my graduate education.

I would like to thank Dr. Lawrence Ziomek for sharing his experience and knowledge throughout this research.

“My religion consists of a humble admiration of the illimitable superior spirit who reveals himself in the slight details we are able to perceive with our frail and feeble mind." - Albert Einstein

THIS PAGE INTENTIONALLY LEFT BLANK

EXECUTIVE SUMMARY

The goal of this thesis was to demonstrate improvements to Synthetic Aperture Sonar (SAS) beamforming algorithms. SAS systems are currently in development to support the Navy's Long-Term Mine Reconnaissance System (LMRS). The LMRS will use a submarine-launched autonomous underwater vehicle to create a synthetic array for high-resolution mine imaging and classification.

Currently, SAS signal processing techniques make various assumptions and simplifications in the determination of the signal propagation ranges and phase shift corrections required for accurate acoustic modeling. These approximate techniques simplify the steering of the beam pattern of the sonar aperture but also unnecessarily introduce errors that affect image quality.

Beamforming techniques have been developed that can exactly determine the parameters required to steer the beam pattern of a sonar array. Using this exact method, acoustic signal propagation in the ocean for a SAS system was simulated. This simulation was conducted using stationary targets to replicate the problem of water-borne mine detection and classification. Water-borne mines include buoyant, tethered, and bottom ocean mines. The primary focus of these simulations was to demonstrate the improvement in SAS beamforming that can be realized through exact propagation range calculation. With exact range estimation, exact phase weights are determined and used to improve array gain.

An analysis of the limitations of the most common approximations is presented. The exact beamforming methods have no restrictions on their application, and this is demonstrated through simulation. The simulation of the propagation of signals from transmitter to target and then to the receiver allows direct comparison of the standard approximate methods with the new exact methods. Estimation of signal propagation range, travel time, angles of incidence and scatter at the target and angles of incidence at the receiver are all improved. Finally, fast Fourier transform beamforming is conducted and the performance of the exact and approximate methods is compared using a simple signal composed of three different sinusoids.

This research demonstrates that simple approximation techniques traditionally used to estimate SAS propagation ranges are not useful in current SAS projects that employ high frequency signals and long target ranges. This research also shows that SAS propagation ranges can be accurately approximated using the binomial approximation propagation model presented in this thesis. Although the binomial approximation propagation model is accurate under most conditions, this model places some restrictions on target range and platform speed. The effects of operating outside the binomial approximation model limits are demonstrated. It is shown that implementation of the exact propagation range method does not significantly add to the complexity of the beamforming algorithm. The exact method introduces no error and places no restrictions on target location and platform speed. Use of the exact propagation model is recommended to allow maximum accuracy and flexibility as SAS systems evolve. Further investigation will determine

the improvements that can be realized by applying the exact time-varying angles of incidence and scatter to the evaluation of target scattering functions.

THIS PAGE INTENTIONALLY LEFT BLANK

I. INTRODUCTION

This chapter provides an overview of synthetic aperture sonar concepts. The modeling framework used to simulate signal propagation through the ocean medium is also introduced.

A. SYNTHETIC APERTURE SONAR

Synthetic Aperture Sonar (SAS) systems attempt to exploit the benefits that can be obtained from very long sonar arrays while maintaining the actual physical size of the array to be relatively small. This is an attractive technique because it would allow deployment of Unmanned Underwater Vehicles (UUV) to detect, localize and classify mines in the littoral environment. Vehicle size is limited by the launching capability of the controlling ship or aircraft and a need to conduct covert surveillance and mine hunting. The high resolution necessary for classification of mines, however, requires a very long array. One of the most attractive ways to satisfy these competing requirements is through aperture synthesis.

The principle of aperture synthesis is the coherent combination of successive returns from a transmitter located on a moving platform. This coherent processing of received echoes provides enhanced resolution in azimuth compared with standard sonar systems. The key to SAS signal processing is estimating the time delay of each received pulse while compensating for motion of the array and the target. This process can be thought of as focusing of

the phase history of the signal [1]. Traditional sonar arrays use multiple transmit and receive elements to simultaneously transmit and then simultaneously receive acoustic signals. Conversely, synthetic aperture arrays synthesize the array by processing the output electrical signals of a single transmit and receive element or group of elements as the element travels through the medium. A comparison of the traditional array and a synthetic aperture can be seen in Figure 1.

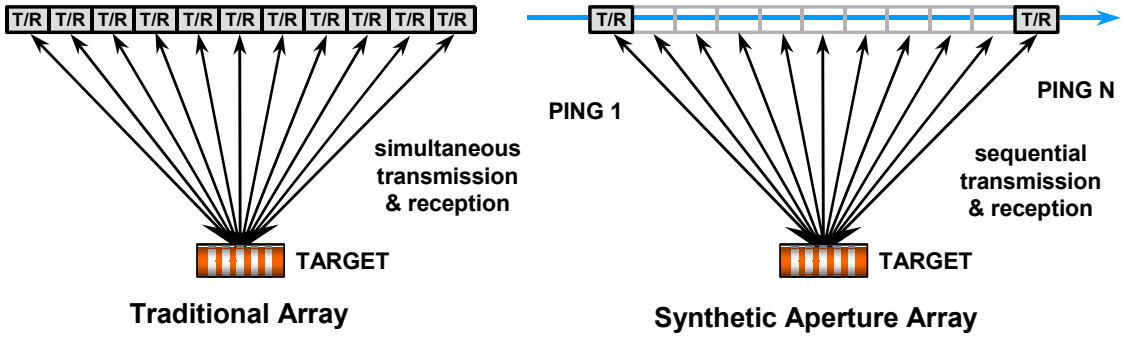

Figure 1. Traditional and synthetic aperture arrays [After Ref. 2].

SAS systems are similar to Synthetic Aperture Radar (SAR) systems in many respects but SAS signal processing provides some unique challenges. SAR systems have wider absolute bandwidth and higher carrier-to-bandwidth ratio, or quality factor Q. The high Q nature of SAR dictates that typical motion and range estimation errors have little effect on the echo. The errors result in a shift of a few centimeters on a signal envelope of a few meters. In contrast, SAS motion and range estimation errors of a few centimeters result in a shift of the target envelope that

is also on the order of a few centimeters [3]. The strong dependence of SAS systems on accurate range and motion estimation is the focus of the research presented in this thesis.

Several other challenges must be considered when designing a SAS system. The speed of the platform must be high enough to maintain control of the submerged vehicle but slow enough to prevent undersampling of the target area. As described above, SAS system resolution can be significantly degraded by residual motion errors of the transmit and receive platforms.

B. THE OCEAN AS A LINEAR, TIME-VARIANT, SPACE-VARIANT FILTER

Computer simulation of acoustic ray propagation in an unbounded ocean medium was the primary means of evaluating the exact propagation equations and comparing these techniques to common approximations. The mathematical framework used for these simulations models the ocean as a linear, time-variant, space-variant filter. The theory, methods, and derivation of this linear systems approach to acoustic field theory are contained in [4]. A block diagram model of pulse propagation is shown in Figure 2. The simulations conducted in this thesis focus on determination of exact and approximate acoustic propagation paths included in the complex frequency response of the ocean medium. The complex frequency response of the ocean medium at time t, position $\boldsymbol{r}$, and frequency f due to application of a unit-amplitude impulse at position $\boldsymbol{r}_0$ is $H_M\left(t,\boldsymbol{r}\middle|f,\boldsymbol{r}_0\right)$, as seen in Figure 2.

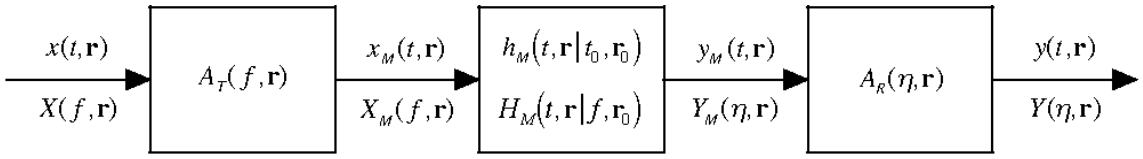

Figure 2. Block diagram model of small-amplitude pulse propagation [From Ref. 5].

Models used for simulation are based on bistatic scattering with a stationary target. This scenario is intended to model the performance of a submerged vehicle using a side scan sonar to image stationary mines. The transmitter and receiver are co-located on the platform. Due to motion of the vehicle the position of the transmitter and receiver is time varying. It is important to note that the vehicle will be in motion during the entire transmit and receive cycle. Some SAS signal-processing algorithms assume that the vehicle is stationary during each transmit and receive cycle and moves only between each cycle [6]. This simplification requires motion compensation to be applied during signal processing and can introduce errors in the image. The models used in this thesis are exact and require no motion compensation. The exact models do, however, assume that the velocity of the platform is constant during transmission and reception of individual pulses.

C. RESEARCH GOALS

This thesis focuses on the direct comparison of exact and approximate signal propagation models as applied to a SAS system employed to image stationary targets. This research validates, through computer simulation, the exact propagation model. The exact model is then used to evalu-

ate errors introduced by approximate methods. The goal of this research is to provide a proven SAS signal-processing algorithm that removes errors due to propagation range, angle, and platform motion estimation. With reduced error, the synthetic aperture array has increased array gain and improved image quality.

D. DOD RELEVANCE

Mine detection and classification is one of the most important challenges faced by the Navy. Simple, inexpensive, effective mines are available to all our potential adversaries. Deployment of water-borne mines by an adversary precludes the introduction of ships or troops into an otherwise unprotected area.

The effectiveness of mine warfare was proven in the 1991 Persian Gulf War. The USS Tripoli sustained 3.5 million dollars in damage after being struck by a 1500 dollar mine. Later in the war, the USS Princeton was disabled by a similar mine. Repairs to the USS Princeton cost 24 million dollars [7]. Battle group commanders are justified in their reluctance to employ assets where the threat of water-borne mines exists.

To address the asymmetric threat of mines, the U.S. Navy is currently developing a Long-Term Mine Reconnaissance System (LMRS). The LMRS is an unmanned underwater vehicle that will use a forward-looking sonar system for mine detection and a side-scan sonar system for localization and classification. The side-scan sonar is used as the transmitter and receiver for a SAS system. This system

provides no risk access to mined waters while collecting information essential to mine hunting operations. A conceptual drawing of the LMRS can be seen in Figure 3.

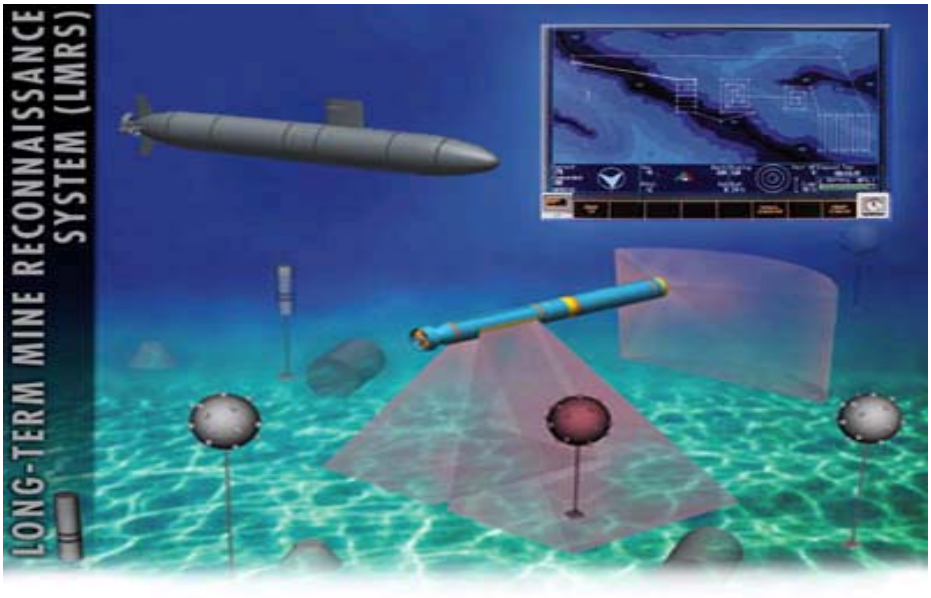

Figure 3. LMRS conceptual drawing [From Ref. 8].

E. SUMMARY

Reliable detection and classification of water-borne mines is an essential capability for the U.S. Navy. SAS systems on UUV's are currently under development to address this challenge. Traditional SAS beamforming algorithms use approximations to calculate acoustic signal propagation ranges and angles of incidence. Exact methods of determining these parameters have been developed and improve system performance. This thesis uses computer simulations of exact and approximate propagation models based on linear systems theory to compare the performance of these methods.

F. THESIS ORGANIZATION

This thesis is organized into five chapters. Chapter I provides an overview of the SAS concept, military relevance of this research, and a general description of the modeling methods and evaluation techniques used for system simulation. An overview of the application of linear systems theory to acoustic propagation modeling is presented in Chapter II. Chapter III introduces the mathematical models used for simulation of SAS as applied to the imaging of stationary water–borne targets. The results of computer simulations designed to compare different methods of estimating acoustic signal propagation ranges and received phase angles are presented in Chapter IV. Finally, Chapter V presents the thesis conclusions and recommendations for future research in SAS signal processing.

The next chapter describes the treatment of the ocean as a linear, time-variant, space-variant filter. The SAS mine-hunting geometry and scattering model are also introduced.

THIS PAGE INTENTIONALLY LEFT BLANK

II. THE OCEAN AS A LINEAR, TIME-VARIANT, SPACE-VARIANT FILTER

This chapter presents an overview of the application of linear systems theory to acoustic propagation modeling.

A. INTRODUCTION

The computer simulations presented in this thesis are based on a linear systems model of the ocean environment. A linear systems approach to acoustic pulse propagation is presented in [4] and [5]. All simulation models in this thesis are based on treatment of the ocean as a linear filter.

Propagation of small amplitude acoustic pulses in the ocean can be described by a linear wave equation. This linear wave equation accurately describes the propagation of acoustic pulses from the source to the discrete point scatterer and from the discrete point scatterer to the receiver. To model this propagation, we treat the ocean as a linear, time-variant, space-variant filter.

B. COMPLEX FREQUENCY RESPONSE OF THE OCEAN

The propagation of small amplitude acoustic pulses through the ocean medium can be described by the linear, three-dimensional, inhomogeneous wave equation, [5]

$$\nabla^2 y_M(t,\mathbf{r}) - \frac{1}{c^2(\mathbf{r})}\frac{\partial^2}{\partial t^2} y_M(t,\mathbf{r}) = x_M(t,\mathbf{r}), \qquad (2.1)$$

where $x_M(t,\mathbf{r})$ is the source distribution at time t and position $\mathbf{r}$ with units of inverse seconds and $y_M(t,\mathbf{r})$ is the velocity potential of the acoustic field at time t and position $\mathbf{r}$ with units of squared meters per second. The vector $\mathbf{r}=(x,y,z)$ describes the location of any point in three-dimensional space. The position dependent speed of sound in meters per second is described by $c(\mathbf{r})$. Note that both the source distribution and the velocity potential are functions of time and position. The time-variant property of the linear filter allows us to model motion of the transmitter, target, and receiver. This ability to accurately model motion of all platforms is essential in SAS modeling where transmitter and receiver motion is used to synthesize the array. This time-variant property also is used to account for changes in the ocean medium with time. The space-variant property allows for the presence of boundaries, discrete point scatterers and spatial variation in ambient density and the speed of sound.

The solution of Eq.(2.1) can be obtained by treating the ocean as a linear, time-variant, space-variant filter. Figure 4 is the linear system block diagram of the ocean as a time-variant, space-variant filter. The input-output relationship is given by [5]

$$y_M(t,\mathbf{r}) = \int_{-\infty}^{\infty}\int_{-\infty}^{\infty} x_M(t_0,\mathbf{r}_0)\,h_M\left(t,\mathbf{r}\,\middle|\,t_0,\mathbf{r}_0\right)dt_0\,d\mathbf{r}_0\,, \qquad (2.2)$$

where $h_M\left(t,\mathbf{r}\,\middle|\,t_0,\mathbf{r}_0\right)$ is the time-variant, space-variant, impulse response (Green's function) of the system. The impulse response $h_M\left(t,\mathbf{r}\,\middle|\,t_0,\mathbf{r}_0\right)$ is the response of the filter at time t

and position $\mathbf{r} = (x, y, z)$ due to application of a unit amplitude impulse at time t_0 and position $\mathbf{r}_0 = (x_0, y_0, z_0)$. The input acoustic signal $x_M(t, \mathbf{r})$ is the source distribution at time t and position $\mathbf{r}$ and $y_M(t, \mathbf{r})$ is output acoustic signal at time t and position $\mathbf{r}$. It is important to realize that Eq.(2.2) is a four-fold integral since $d\mathbf{r}_0 = dx_0\, dy_0\, dz_0$.

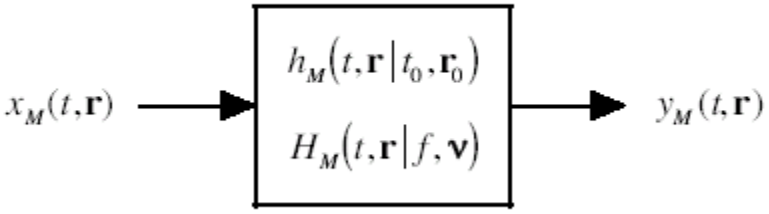

Figure 4. A linear, time-variant, space-variant, ocean medium filter [From Ref. 5].

Figure 4 also shows the time-variant, space-variant, transfer function of the ocean filter $H_M(t, \mathbf{r} | f, \boldsymbol{\nu})$ defined by [5]

$$H_M(t, \mathbf{r} | f, \boldsymbol{\nu}) \triangleq \int_{-\infty}^{\infty} H_M(t, \mathbf{r} | f, \mathbf{r}_0) \exp[+j2\pi \boldsymbol{\nu} \bullet (\mathbf{r} - \mathbf{r}_0)]\, d\mathbf{r}_0, \qquad (2.3)$$

where f represents input frequency components in Hertz and $\boldsymbol{\nu} = (f_X, f_Y, f_Z)$ is a vector representation of the spatial frequencies in cycles per meter in the *X*, *Y*, and *Z* directions, respectively. The time-variant, space-variant, complex frequency response of the ocean at frequency f is [5]

$$H_M(t, \mathbf{r} | f, \mathbf{r}_0) \triangleq \int_{-\infty}^{\infty} h_M(t, \mathbf{r} | t_0, \mathbf{r}_0) \exp[-j2\pi f(t - t_0)]\, dt_0 . \qquad (2.4)$$

The strategy followed in Reference 5 is to first find the time harmonic solution to the linear, inhomogeneous, three-dimensional wave equation. The time harmonic solution is then used to find a pulse solution to the wave equation by using Fourier transform techniques.

The focus of this thesis is on the complex frequency response of the ocean medium, $H_M\left(t,\mathbf{r}\middle|f,\mathbf{r}_0\right)$, as defined by Eq.(2.4). The complex frequency response of the ocean medium integrates the characteristics of the propagation path between transmitter, discrete point scatterer, and receiver. Simulations were conducted using both exact and approximate propagation ranges to account for signal propagation delay as determined by propagation path of the acoustic field.

C. SUMMARY

The ocean medium can be modeled as a linear, time-variant, space-variant, filter. This approach allows us to develop a time-variant, space-variant, complex frequency response of the ocean that accurately describes acoustic signal propagation and therefore provides a solution to the linear, inhomogeneous, wave equation given by equation (2.1). In the next chapter, the complex frequency response of the ocean is derived for the specific case of SAS applied to stationary object detection.

III. MODELING OF BISTATIC SCATTERING FOR SYNTHETIC APERTURE SONAR

This chapter introduces the mathematical model used for simulation of synthetic aperture sonar (SAS) as applied to the imaging of stationary water-borne targets. Several traditional approximations and an exact solution for propagation ranges are introduced and the limitations of each are discussed.

A. INTRODUCTION

The main advantage of a SAS system is the ability to synthesize an extremely long array while maintaining a relatively small actual size of the physical array. Synthetic aperture sonar beamforming and signal processing relies on properly steering and focusing the aperture beam pattern in order to co-phase all the received signals. Due to the effects of motion in the SAS problem, the propagation path from the transmitter to the discrete point scatterer and from discrete point scatterer to the receiver is time varying. Traditionally, simple approximations are used to determine these propagation ranges and angles of incidence and scatter. This chapter introduces the exact bistatic scattering model for SAS systems presented in [9] as well as some common approximations used when modeling acoustic signal propagation in SAS systems.

B. BISTATIC SCATTERING MODEL

1. Assumptions

The focus of this section is to develop the complex frequency response of the ocean for a SAS system with stationary targets. In the binomial approximation models and the exact propagation models described in this thesis, the speed of sound and the ambient density of the ocean are treated as constants. This allows us to treat the ocean medium as homogeneous. As a result, sound rays will travel in straight lines from the transmitter to the discrete point scatterer and from the discrete point scatterer to the receiver. Propagation models involving surface and bottom interactions can be developed in an identical manner to those presented for propagation between the transmitter and discrete point scatterer and discrete point scatterer and receiver [9].

The transmitter and receiver velocity vectors are assumed to be constant only during the transmission and reception of the acoustic pulse. The platform may change its speed at any time in any direction between transmission and reception and between cycles. This feature eliminates the need for motion compensation typically applied to most SAS signal processing algorithms. The binomial approximation and exact propagation models assume only that the position and velocity vectors of the transmitter and receiver can be determined during signal transmission and reception. Determination of the vehicle velocity vector is not a trivial problem, however, and accurate determination of vehicle

position is an area of extensive research in SAS signal processing and vehicle design [1, 10, 11].

In order to allow comparison of the various methods of propagation range determination, the scattering function of the discrete point scatterer, $g_1\left(f, \hat{n}'_{0,1}, \hat{n}''_{1,2}\right)$, is assumed to be unity.

2. Propagation Geometry

We begin our development of the complex frequency response of the ocean by defining the velocity vectors for the transmitter, $\mathbf{V}_0$, the discrete point scatterer, $\mathbf{V}_1$, and the receiver, $\mathbf{V}_2$. These velocity vectors are given by [9]

$$\mathbf{V}_0 = V_0 \hat{n}_{V_0}, \tag{3.1}$$

$$\mathbf{V}_1 = V_1 \hat{n}_{V_1}, \tag{3.2}$$

and

$$\mathbf{V}_2 = V_2 \hat{n}_{V_2}, \tag{3.3}$$

where V_0, V_1, and V_2 are the speeds in meters per second of the transmitter, discrete point scatterer, and receiver, respectively. The dimensionless unit vectors $\hat{n}_{V_0}$, $\hat{n}_{V_1}$, and $\hat{n}_{V_2}$ define the directions of $\mathbf{V}_0$, $\mathbf{V}_1$, and $\mathbf{V}_2$, respectively. Velocity vectors given by Eqs.(3.1) through (3.3) are constant as discussed in Section III.B.1. Motion is considered to begin at time $t = t_m$.

The time-varying geometry of the scattering model is modified using relative velocity vectors to allow the transmitter and the discrete point scatterer to be treated

as being motionless. The velocity vector of the discrete point scatterer relative to the velocity vector of the transmitter in the direction of the velocity vector of the discrete point scatterer $\hat{n}_{V_1}$, is [9]

$$\mathbf{V}_{1,0} = \mathbf{V}_1 - \left(\hat{n}_{V_1} \bullet \mathbf{V}_0\right)\hat{n}_{V_1} = \left[V_1 - V_0\left(\hat{n}_{V_1} \bullet \hat{n}_{V_0}\right)\right]\hat{n}_{V_1} . \tag{3.4}$$

The initial propagation model allows for motion of the discrete point scatterer, so we define a relative velocity vector, $\mathbf{V}_{2,1}$. The vector $\mathbf{V}_{2,1}$ is the velocity vector of the receiver relative to the velocity vector of the discrete point scatterer in the direction of the velocity vector of the receiver $\hat{n}_{V_2}$ and is given by [9]

$$\mathbf{V}_{2,1} = \mathbf{V}_2 - \left(\hat{n}_{V_2} \bullet \mathbf{V}_1\right)\hat{n}_{V_2} = \left[V_2 - V_1\left(\hat{n}_{V_2} \bullet \hat{n}_{V_1}\right)\right]\hat{n}_{V_2} . \tag{3.5}$$

The position vectors from the origin to the transmitter, discrete point scatterer, and receiver when motion begins at $t = t_m$ are given by $\mathbf{r}_0 = (x_0, y_0, z_0)$, $\mathbf{r}_1 = (x_1, y_1, z_1)$, and $\mathbf{r}_2 = (x_2, y_2, z_2)$, respectively. Using these position vectors, we can further define the position vector from the transmitter to the discrete point scatterer as [9]

$$\mathbf{r}_{0,1} = \mathbf{r}_1 - \mathbf{r}_0 \tag{3.6}$$

and the position vector from the discrete point scatterer to the receiver as [9]

$$\mathbf{r}_{1,2} = \mathbf{r}_2 - \mathbf{r}_1 . \tag{3.7}$$

The dimensionless unit vectors from source to discrete point scatterer and from discrete point scatterer to receiver are [9]

$$\hat{n}_{0,1} = \frac{\mathbf{r}_{0,1}}{\left|\mathbf{r}_{0,1}\right|} \tag{3.8}$$

and

$$\hat{n}_{1,2} = \frac{\mathbf{r}_{1,2}}{\left|\mathbf{r}_{1,2}\right|}, \tag{3.9}$$

respectively. The ranges in meters from the transmitter to discrete point scatterer and from the discrete point scatterer to receiver are given by [9]

$$r_{0,1} = \left|\mathbf{r}_{0,1}\right| \tag{3.10}$$

and

$$r_{1,2} = \left|\mathbf{r}_{1,2}\right|, \tag{3.11}$$

respectively. This bistatic scattering geometry is shown in Figure 5.

It is now important to define the parameters of our model with respect to the time instance when the acoustic field is first incident upon the discrete point scatterer and the time instance when the acoustic field is first incident upon the receiver. The transmitted acoustic field is first incident upon the discrete point scatterer at some time t' seconds where $t' > t_m$. This allows us to define the time difference from transmission of the acoustic field to first incidence upon the discrete point scatterer as [9]

$$\Delta t' = t' - t_m, \quad t' > t_m . \tag{3.12}$$

Similarly, the time instant when the scattered acoustic field is first incident upon the receiver is $t > t' > t_m$. The

time difference between t' and first incidence of the acoustic field upon the receiver is given by [9]

$$\Delta t'' = t - t', \quad t > t' > t_m \,. \tag{3.13}$$

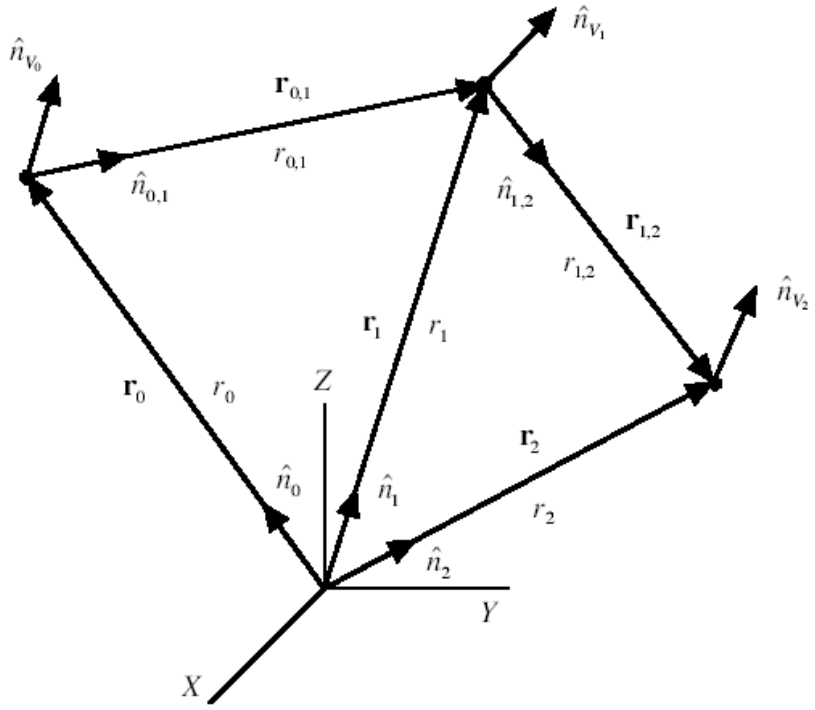

Figure 5. Bistatic scattering geometry when motion begins at time $t = t_m$ seconds. Point 0, $P_0(\mathbf{r}_0)$, is the transmitter; point 1, $P_1(\mathbf{r}_1)$, is the discrete point scatterer; and point 2, $P_2(\mathbf{r}_2)$, is the receiver. All three platforms are in motion [From Ref. 5].

By referring to Figure 6 we can express the position vector from the point source to the discrete point scatterer at time t' as $\mathbf{r}'_{0,1}$ and the position vector from the

discrete point scatterer to the receiver at time t as $\mathbf{r}''_{1,2}$. The position vector from the origin to the discrete point scatterer at time t' is $\mathbf{r}'_1$. The position vector from the origin to the receiver at time t is $\mathbf{r}''_2$.

3. Velocity Potential and Complex Frequency Response

Our goal is to develop an expression for the complex frequency response of the ocean in order to compare different methods for estimation of propagation range from transmitter to discrete point scatterer and from discrete point scatterer to receiver. Prediction of the propagation ranges $\left|\mathbf{r}'_{0,1}\right|$ and $\left|\mathbf{r}''_{1,2}\right|$ will allow us to correctly steer and focus the beam pattern of our synthetic array resulting in the co-phasing of the output electrical signals at the different receiver locations. Once a model for the complex frequency response is developed, we can predict the acoustic field (velocity potential) at the receiver.

When the transmitted acoustic field is first incident upon the discrete point scatterer at time t', the position vector from the transmitter to the discrete point scatterer is given by [9]

$$\mathbf{r}'_{0,1} = \mathbf{r}_{0,1} + \Delta t' \, \mathbf{V}_{1,0} \, . \qquad (3.14)$$

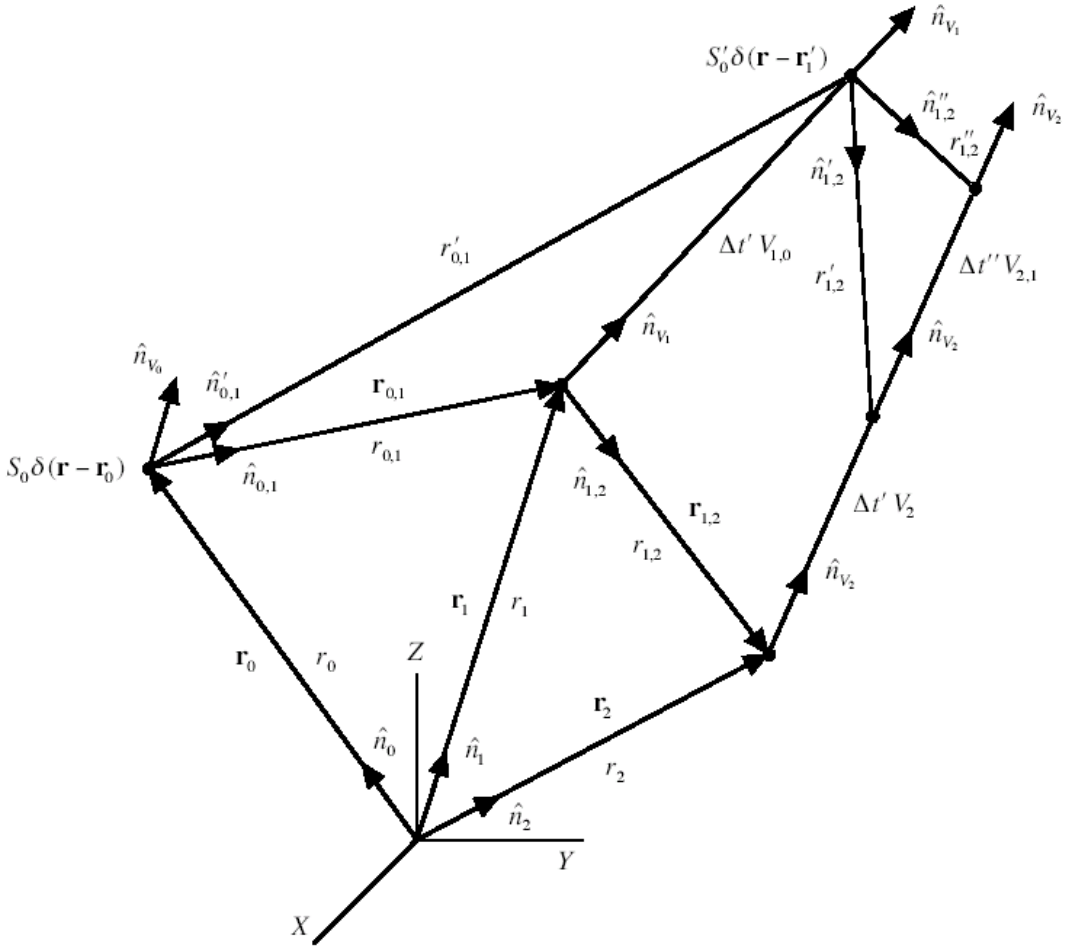

Figure 6. Bistatic scattering geometry when the transmitted acoustic field is first incident upon the discrete point scatterer at time t' seconds and when the scattered acoustic field is first incident upon the receiver at time t seconds where $t > t' > t_m$. Point 0, $P_0(\mathbf{r}_0)$, is the transmitter; point 1, $P_1(\mathbf{r}_1)$, is the discrete point scatterer, and point 2, $P_2(\mathbf{r}_2)$, is the receiver. All three platforms are in motion [From Ref. 5].

Recall that we are modeling the propagation of the acoustic field through the ocean as transmission through a linear time-variant, space-invariant filter. Therefore, the acoustic field incident upon the discrete point scatterer at time t' and position $\mathbf{r}_1' = \left(x_1', y_1', z_1'\right)$ is [9]

$$y_M\left(t', \mathbf{r}_1'\right) = S_0 H_M\left(t', \mathbf{r}_{0,1}' \middle| f\right) \exp\left(+j2\pi f t'\right), \quad t' > t_m \tag{3.15}$$

where

$$H_M\left(t', \mathbf{r}_{0,1}' \middle| f\right) = -\frac{\exp\left(-jk\left|\mathbf{r}_{0,1}'\right|\right)}{4\pi\left|\mathbf{r}_{0,1}'\right|} \tag{3.16}$$

is the time-variant, space-invariant, complex frequency response of the ocean at frequency f hertz. The source strength S_0 is given in cubic meters per second and k is the wavenumber in radians per meter given by

$$k = 2\pi f / c = 2\pi / \lambda \,. \tag{3.17}$$

An identical method is used in [9] to develop an expression for the acoustic field incident upon the receiver at time t. The position vector between the discrete point scatterer and the receiver at time $t > t' > t_m$ is given by [9]

$$\mathbf{r}_{1,2}'' = \mathbf{r}_{1,2} + \Delta t'\left(\mathbf{V}_2 - \mathbf{V}_{1,0}\right) + \Delta t''\mathbf{V}_{2,1} \,. \tag{3.18}$$

The acoustic field (velocity potential) incident upon the receiver at time $t > t' > t_m$ is [9]

$$y_M\left(t, \mathbf{r}_2''\right) = S_0 H_M\left(t, \mathbf{r}_2'' \middle| f, \mathbf{r}_0\right) \exp\left(+j2\pi f t\right), \quad t > t' > t_m \tag{3.19}$$

where

$$H_M\left(t,\mathbf{r}_2''\middle|f,\mathbf{r}_0\right)=H_M\left(t',\mathbf{r}_{0,1}'\middle|f\right)g_1\left(f,\hat{n}_{0,1}',\hat{n}_{1,2}''\right)H_M\left(t,\mathbf{r}_{1,2}''\middle|f\right)$$
$$=g_1\left(f,\hat{n}_{0,1}',\hat{n}_{1,2}''\right)\frac{\exp\left[-jk\left(\left|\mathbf{r}_{0,1}'\right|+\left|\mathbf{r}_{1,2}''\right|\right)\right]}{16\pi^2\left|\mathbf{r}_{0,1}'\right|\left|\mathbf{r}_{1,2}''\right|}. \qquad (3.20)$$

The complex scattering function of the discrete point scatterer, $g_1\left(f,\hat{n}_{0,1}',\hat{n}_{1,2}''\right)$, is dependent upon frequency and upon the angles of incidence and scatter. For simplicity, this function is assumed to be unity in this thesis so that we may independently investigate the phase term in Eq.(3.20).

C. PROPAGATION RANGE DETERMINATION

The key to proper co-phasing of the output electrical signals from the SAS array is estimation of the received phase of the acoustic field incident upon the receiver. Examination of Eq.(3.20) reveals that the phase term, $\exp\left[-jk\left(\left|\mathbf{r}_{0,1}'\right|+\left|\mathbf{r}_{1,2}''\right|\right)\right]$, depends directly on frequency and the magnitude of the position vectors $\mathbf{r}_{0,1}'$ and $\mathbf{r}_{1,2}''$. It is in the solution for these time-varying ranges that this thesis is focused. Accurate determination of the propagation range of the acoustic signal is especially important in recent SAS projects such as the Long-Term Mine Reconnaissance System (LMRS) where relatively high carrier frequencies will be used to increase image resolution. Small errors in propagation range estimation can introduce large errors in signal phase estimation at the receiver, significantly degrading the array performance.

1. The Stop-and-Hop Approximation and the Moving Receiver Correction

One approach to estimation of propagation ranges is to assume that the transmitter and receiver are stationary during signal transmission and reception. This assumption is acceptable for many synthetic aperture radar (SAR) systems, but due to the slow propagation speed of acoustic waves in water relative to electromagnetic waves in air, this assumption is invalid for a SAS system imaging targets at any significant range [6]. An initial correction may be applied by compensating for the motion of the receiver in the time interval between signal transmission and signal reception. A method for received phase correction due to a moving receiver is presented in [6]. Figure 7 shows the geometry involved in this correction. The initial range from transmitter to target is R_1. The initial range from target to receiver is R_2. The distance traveled by the receiver during signal propagation is Vt' where V is the vehicle speed and t' is the total propagation time between transmission and reception of the acoustic signal. The propagation time t' is an estimation of the total propagation time from transmitter to target and from target to receiver based on a reference range to the scene center. The range R_3 describes the range from target to receiver at time t'. Each received acoustic signal is multiplied by the phase correction term [6]

$$\exp\left(+j\frac{\omega_0}{c}\Delta\hat{R}\right), \tag{3.21}$$

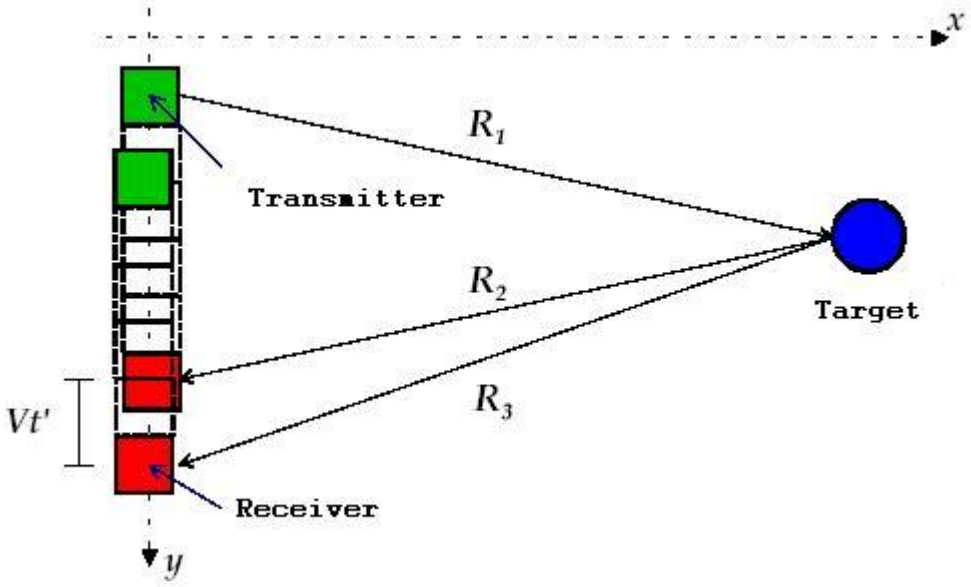

Figure 7. The moving receiver correction for the stop-and-hop geometry [After Ref. 6].

where

$$\Delta\hat{R} = R_3 - R_2 \,. \tag{3.22}$$

Compensating for the motion of the receiver during signal propagation does remove some error inherent in the stop-and-hop assumption but several additional factors are not considered. The motion of the transmitter and receiver *during* signal transmission and reception is ignored. In addition, the vehicle velocity vector is assumed to be constant for the entire duration of signal propagation. This correction further assumes that the total propagation time, t' in Figure 7, from transmitter to target and target to receiver can be approximated by calculating the propagation time to some reference range, R_0, such that [6]

$$t' = \frac{2R_0}{c} \,. \tag{3.23}$$

The reference range, R_0, is the range to the center of the image area of the SAS system [6]. Throughout the remainder of this thesis, the moving receiver correction is applied to the stop-and-hop model and referred to as the stop-and-hop approximation model.

We can define the stop-and-hop model presented in [6] in terms of the bistatic scattering model presented in Section III.B of this thesis. The range from transmitter to discrete point scatterer is given by

$$R_1 = \left|\mathbf{r}_1 - \mathbf{r}_0\right|, \tag{3.24}$$

where $\mathbf{r}_1$ and $\mathbf{r}_0$ are the position vectors from the coordinate system origin to the discrete point scatterer and transmitter, respectively (see Fig. 5). The time-varying range from discrete point scatterer to receiver is given by

$$R_3(t) = \left|\mathbf{r}_2(t) - \mathbf{r}_1\right|, \quad t > t', \tag{3.25}$$

where $\mathbf{r}_2(t)$ is the time-varying range from the coordinate system origin to the receiver given by

$$\mathbf{r}_2(t) = \mathbf{r}_2(t') + \mathbf{V}t, \quad t > t'. \tag{3.26}$$

The vector $\mathbf{V}$ is the velocity vector of the receiver, and t' is given by Eq.(3.23).

2. The Binomial Approximation Method

The magnitude of the position vectors $\mathbf{r}'_{0,1}$ and $\mathbf{r}''_{1,2}$ can be approximated by using the binomial expansion presented in [5]. The magnitude of the position vector from the trans-

mitter to the discrete point scatterer at time t' can be rewritten as [5]

$$\left|\mathbf{r}'_{0,1}\right| = r_{0,1}\sqrt{1+b} \approx r_{0,1}\left(1+\frac{b}{2}-\frac{b}{8}+\cdots\right), \quad |b|<1 \tag{3.27}$$

where

$$b = 2\frac{V_{1,0}\Delta t'}{r_{0,1}}\left[\left(\hat{n}_{0,1}\bullet\hat{n}_{V_1}\right)+\frac{1}{2}\frac{V_{1,0}\Delta t'}{r_{0,1}}\right]. \tag{3.28}$$

Recall that in our bistatic scattering model, t' is the time instant when the transmitted acoustic field is first incident upon the discrete point scatterer and that $t' > t_m$. For the case of a SAS system imaging a *stationary* target,

$$\mathbf{V}_1 = \mathbf{0}. \tag{3.29}$$

Therefore, $\mathbf{V}_{1,0}$ given by Eq.(3.4) is undefined. As a result,

$$\mathbf{V}_{1,0} = \mathbf{0} \tag{3.30}$$

and

$$\left|\mathbf{V}_{1,0}\right| = V_{1,0} = 0. \tag{3.31}$$

In this case, b given by Eq.(3.28) is equal to zero and Eq.(3.27) reduces to

$$\left|\mathbf{r}'_{0,1}\right| = r_{0,1}, \tag{3.32}$$

which is exact.

The binomial approximation can also be applied to the estimation of $\left|\mathbf{r}''_{1,2}\right|$. The range $\left|\mathbf{r}''_{1,2}\right|$ can be written as [5]

$$\left|\mathbf{r}''_{1,2}\right| = r_{1,2}\sqrt{1+b} \approx r_{1,2}\left(1+\frac{b}{2}-\frac{b^2}{8}+\cdots\right), \quad |b|<1 \tag{3.33}$$

where

$$b = \frac{2}{r_{1,2}}\left\{\left[\hat{n}_{1,2}\bullet\left(\mathbf{V}_2-\mathbf{V}_{1,0}\right)\right]\Delta t' + \left(\hat{n}_{1,2}\bullet\mathbf{V}_{2,1}\right)\Delta t''\right\}. \tag{3.34}$$

The expression for b can be simplified using Eqs.(3.29) and (3.30) for the stationary target. Thus, Eq.(3.5) reduces to

$$\mathbf{V}_{2,1} = \mathbf{V}_2 \tag{3.35}$$

and Eq.(3.34) can be rewritten as

$$b = \frac{2}{r_{1,2}}\left\{\left(\Delta t' + \Delta t''\right)\left(\hat{n}_{1,2}\bullet\mathbf{V}_2\right)\right\}. \tag{3.36}$$

Using Eqs.(3.12) and (3.13),

$$\Delta t' + \Delta t'' = t' - t_m + t - t' = t - t_m = \Delta t\,. \tag{3.37}$$

The expression for b now reduces to

$$b = \frac{2}{r_{1,2}}\left\{\Delta t\left(\hat{n}_{1,2}\bullet\mathbf{V}_2\right)\right\}. \tag{3.38}$$

Equation (3.33) is only valid if $|b|<1$. Note that

$$\left|\hat{n}_{1,2}\bullet\mathbf{V}_2\right| \le \left|\mathbf{V}_2\right|. \tag{3.39}$$

Now, if we impose the more stringent criterion that

$$\frac{2\left|\mathbf{V}_2\right|\Delta t}{r_{1,2}} \le 0.1, \tag{3.40}$$

then the binomial approximation can be simplified by using only the first two terms of Eq.(3.33). Doing so yields

$$\left|\mathbf{r}''_{1,2}\right| \approx r_{1,2} + \left[\hat{n}_{1,2} \bullet \left(\mathbf{V}_2 - \mathbf{V}_{1,0}\right)\right]\Delta t' + \left(\hat{n}_{1,2} \bullet \mathbf{V}_{2,1}\right)\Delta t'' \,. \tag{3.41}$$

Equation (3.41) can be further simplified using Eqs.(3.30), (3.35), and (3.37) such that

$$\left|\mathbf{r}''_{1,2}\right| \approx r_{1,2} + \left(\hat{n}_{1,2} \bullet \mathbf{V}_2\right)\Delta t \,. \tag{3.42}$$

3. Exact Propagation Range Method

Reference 9 presents a method for determining the time-varying propagation ranges $\left|\mathbf{r}'_{0,1}(t)\right|$ and $\left|\mathbf{r}''_{1,2}(t)\right|$ exactly for the general case of bistatic scattering when all three platforms (transmitter, target, and receiver) are in motion and for the special case of a SAS system imaging a stationary target. The constant value of range from transmitter to discrete point scatterer when the transmitted acoustic field is first incident upon the discrete point scatterer at time instant $t' > t_m$ is given by [9]

$$\left|\mathbf{r}'_{0,1}\right| = r_{0,1} \,. \tag{3.43}$$

The constant value of range between discrete point scatterer and the receiver when the scattered field is first incident upon the receiver at time instant $t > t' > t_m$ is given by [9]

$$\left|\mathbf{r}''_{1,2}\right| = \frac{B_0 \pm \sqrt{B_0^{\,2} + 4A_0C_0}}{2A_0} \,, \tag{3.44}$$

where

$$A_0 = 1 - \frac{V_0^2}{c^2} \,, \tag{3.45}$$

$$B_0 = 2r_{1,2}\frac{(\hat{n}_{1,2} \bullet \mathbf{V}_0)}{c} + 2r_{0,1}\frac{V_0^2}{c^2}, \tag{3.46}$$

and

$$C_0 = r_{0,1}^2\frac{V_0^2}{c^2} + 2r_{0,1}r_{1,2}\frac{(\hat{n}_{1,2} \bullet \mathbf{V}_0)}{c} + r_{1,2}^2 . \tag{3.47}$$

The time-varying propagation ranges are given by [9]

$$\left|\mathbf{r}''_{1,2}(t)\right| = \left[r_{1,2}^2 + 2r_{1,2}(\hat{n}_{1,2} \bullet \mathbf{V}_0)\Delta t + V_0^2(\Delta t)^2\right]^{1/2}, \qquad t \geq t_m + \tau, \tag{3.48}$$

and

$$\left|\mathbf{r}'_{0,1}(t)\right| = c\Delta t - \left|\mathbf{r}''_{1,2}(t)\right|, \qquad t \geq t_m + \tau, \tag{3.49}$$

where

$$\tau = \frac{\left|\mathbf{r}'_{0,1}\right|}{c} + \frac{\left|\mathbf{r}''_{1,2}\right|}{c} \tag{3.50}$$

is the time delay in seconds or the amount of time it takes for the transmitted acoustic signal to begin to appear at the receiver after motion begins at time instant t_m, and

$$\Delta t = t - t_m, \quad t \geq t_m + \tau . \tag{3.51}$$

D. SUMMARY

Accurate estimation of the propagation range from the transmitter to target and from target to receiver is essential to the proper co-phasing of the output electrical signals from the different receiver locations. The traditional stop-and-hop method, corrected for receiver motion, can be used to estimate propagation ranges. Alternately, the propagation ranges can be determined using the bistatic

scattering model presented in this chapter. The propagation ranges $\left|\mathbf{r}'_{0,1}(t)\right|$ and $\left|\mathbf{r}''_{1,2}(t)\right|$ can be estimated using a binomial approximation or calculated exactly. The next chapter presents the results of computer simulations used to compare the accuracy of the stop-and-hop approximation, binomial approximation, and the exact propagation range calculation methods.

IV. PROPAGATION RANGE AND RECEIVED PHASE ANGLE ESTIMATION COMPARISON

This chapter presents the results of computer simulations designed to compare different methods of estimating acoustic signal propagation ranges and received phase angles for a SAS system imaging a stationary target. Simulation results of the receiver output electrical signals for a SAS array with Fast Fourier Transform (FFT) beamforming and various propagation range estimation methods are also presented.

A. INTRODUCTION

1. Method of Evaluation

Accurate estimation of the propagation range from the transmitter to the discrete point scatterer and from the discrete point scatterer to the receiver is essential to properly co-phase the output electrical signals in the SAS system. Using the models presented in Chapter III, the simulations presented in this chapter compare the propagation ranges and received phase angles computed using the binomial approximation method and stop-and-hop approximation method to the exact propagation ranges and exact received phase angles. Comparisons are based on the percent error in range from transmitter to discrete point scatterer, percent error in range from discrete point scatterer to receiver, and percent error in the estimation of the phase of the signal incident upon the receiver. All simulations were conducted using MATLAB version 6.0.

Comparisons of propagation range and received phase estimation methods are performed for a single transmit/receive cycle. The propagation range error for the time-varying range from transmitter to discrete point scatterer is given by

$$\left|\mathbf{r}'_{0,1}(t)\right|_{Exact} - \left|\mathbf{r}'_{0,1}(t)\right|_{Approx} . \tag{4.1}$$

Similarly, the propagation range error for the time-varying range from discrete point scatterer to receiver is given by

$$\left|\mathbf{r}''_{1,2}(t)\right|_{Exact} - \left|\mathbf{r}''_{1,2}(t)\right|_{Approx} . \tag{4.2}$$

The percent range error for the time-varying range from transmitter to discrete point scatterer is given by

$$\frac{\left|\mathbf{r}'_{0,1}(t)\right|_{Exact} - \left|\mathbf{r}'_{0,1}(t)\right|_{Approx}}{\left|\mathbf{r}'_{0,1}(t)\right|_{Exact}} \times 100\% . \tag{4.3}$$

The percent range error for the time-varying range between discrete point scatterer and receiver is given by

$$\frac{\left|\mathbf{r}''_{1,2}(t)\right|_{Exact} - \left|\mathbf{r}''_{1,2}(t)\right|_{Approx}}{\left|\mathbf{r}''_{1,2}(t)\right|_{Exact}} \times 100\% . \tag{4.4}$$

Finally, the phase in radians of the acoustic signal incident upon the receiver is given by

$$\theta(t) = \frac{2\pi}{\lambda}\left(\left|\mathbf{r}'_{0,1}(t)\right| + \left|\mathbf{r}''_{1,2}(t)\right|\right) \tag{4.5}$$

and the percent phase error is given by

$$\frac{\theta(t)_{Exact} - \theta(t)_{Approx}}{\theta(t)_{Exact}} \times 100\% . \tag{4.6}$$

2. Simulation Parameters

The computer simulations developed for this thesis simulate vehicle motion in any direction in an unbounded, homogeneous, ocean medium. Although the simulation places no restrictions on target location, the target is always assumed to be at some depth below the transmit/receive platform. Unless otherwise noted, the vehicle begins motion at time t_m at the origin of the coordinate system and is imaging a target forward of the beam ($\phi = 45^\circ$) at a range, R (see Fig. 8). For simplicity, platform motion is along the positive Z axis.

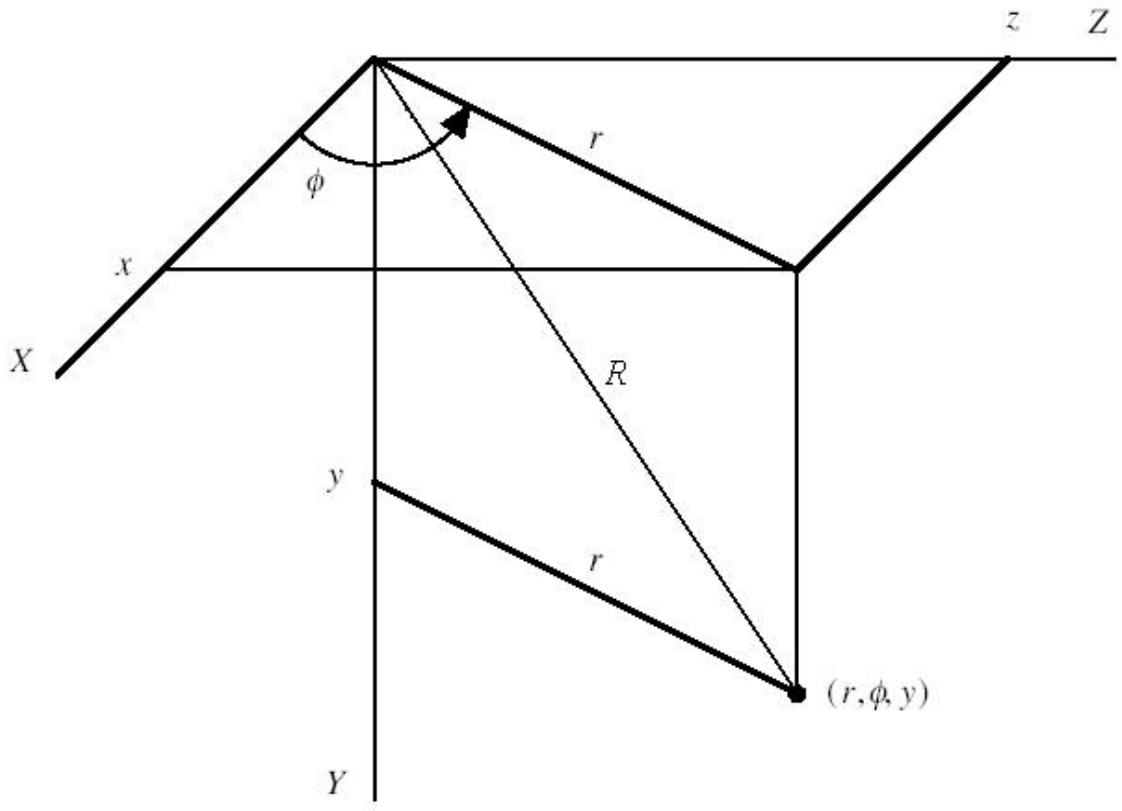

Figure 8. SAS simulation geometry [After Ref. 5].

Propagation ranges are calculated with the equations presented in III.C.1 through III.C.3 using the assumptions presented in III.B.1.

The platform speeds and target ranges used for comparison are similar to those that have been specified for the Navy's LMRS system [2]. The LMRS side-scan sonar system is used to synthesize the SAS array. The side-scan sonar array covers both sides of the six-foot long LMRS platform, allowing independent imaging on both the port and starboard sides of the vehicle. The vehicle is designed to travel between 3 and 7 knots [2]. The minimum speed is based on maintaining maneuverability. The maximum speed is set to ensure adequate sampling of the target area. Figure 9 shows the relationship between physical array length, platform speed, and maximum range.

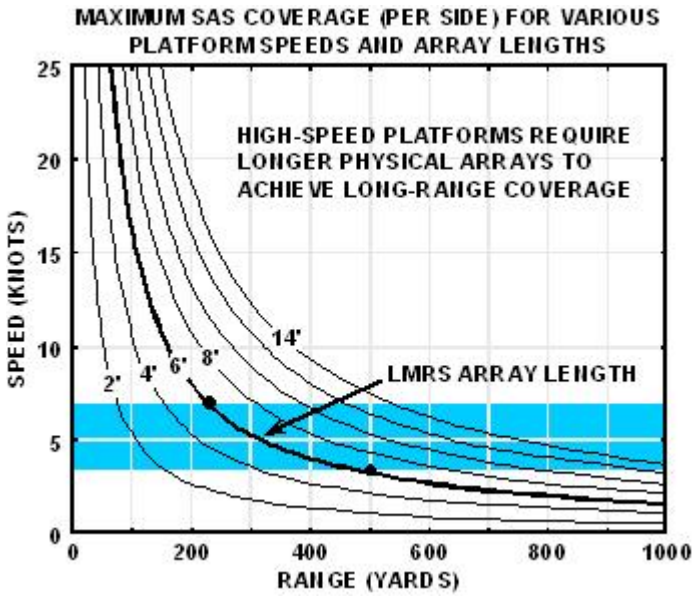

Figure 9. LMRS Range and Speed limitations [From Ref. 2].

3. FFT Beamforming

The simulations presented in the next section compare the accuracy of the approximate stop-and-hop propagation range method and the approximate binomial approximation propagation range method for each transmit/receive cycle of the platform. To provide further comparison and to better analyze the effects of approximation errors on SAS systems, the propagation range calculations from the stop-and-hop approximation, binomial approximation, and exact methods are used to estimate the phase weights in a Fast Fourier Transform (FFT) beamforming algorithm.

To independently investigate the performance of each method due to phase errors, we assume the scattering function of the target is unity as discussed in Sections III.B.1 and III.B.3. We also neglect the propagation range term, $16\pi^2 \left|\mathbf{r}'_{0,1}\right| \left|\mathbf{r}''_{1,2}\right|$, in the denominator of Eq.(3.20). Neglecting this *amplitude* factor allows us to focus on the effect of propagation range error on received phase prediction.

Three simple sinusoids, each at a different frequency, are used to simulate acoustic propagation. As a result, Eq.(3.19) can be expressed as

$$y_M\left(t, \mathbf{r}''_2(t)\right) = \sum_{i=1}^{3} \exp\left[-jk_i\left(\left|\mathbf{r}'_{0,1}(t)\right| + \left|\mathbf{r}''_{1,2}(t)\right|\right)\right] \exp\left(j2\pi f_i t\right), \qquad (4.7)$$

where

$$k_i = \frac{2\pi f_i}{c} \qquad (4.8)$$

is the wavenumber for each different frequency and $f_1 = 10$ kHz, $f_2 = 20$ kHz, and $f_3 = 30$ kHz.

We assume that the output electrical signal of the receiver is directly proportional to the acoustic field incident upon the receiver. Therefore,

$$y\left(t,\mathbf{r}_2''(t)\right)=y_M\left(t,\mathbf{r}_2''(t)\right). \tag{4.9}$$

We now describe the FFT beamforming algorithm used in this thesis and is shown in Fig. 10. FFT beamforming is accomplished by first taking the time-domain Fourier transform of the output electrical signals at the receiver at different positions as the SAS system images a target at a known location. These signals are simulated using the exact propagation model to compute the acoustic signal incident upon the array given by Eq.(4.7), where $\left|\mathbf{r}_{0,1}'(t)\right|$ and $\left|\mathbf{r}_{1,2}''(t)\right|$ are given by Eqs.(3.49) and (3.48), respectively. The resulting output electrical signals are given by Eq.(4.9). These exact electrical signals are then phase weighted with phase weights computed using one of the approximate methods.

These approximate phase weights are computed by first determining the acoustic field incident upon the receiver using Eq.(4.7), where the values for $\left|\mathbf{r}_{0,1}'(t)\right|$ and $\left|\mathbf{r}_{1,2}''(t)\right|$ are computed using either the binomial approximation method or the stop-and hop approximation method. The approximate stop-and-hop values for $\left|\mathbf{r}_{0,1}'(t)\right|$ and $\left|\mathbf{r}_{1,2}''(t)\right|$ are given by Eqs.(3.24) and (3.25), respectively. The approximate binomial approximation values for $\left|\mathbf{r}_{0,1}'(t)\right|$ and $\left|\mathbf{r}_{1,2}''(t)\right|$ are given by Eqs.(3.32) and (3.42), respectively. The negative of the phase spectrum of the time-domain Fourier transform of the

output electrical signals given by Eq.(4.9) determine the appropriate approximate phase weights to use to phase weight the receiver output electrical signals.

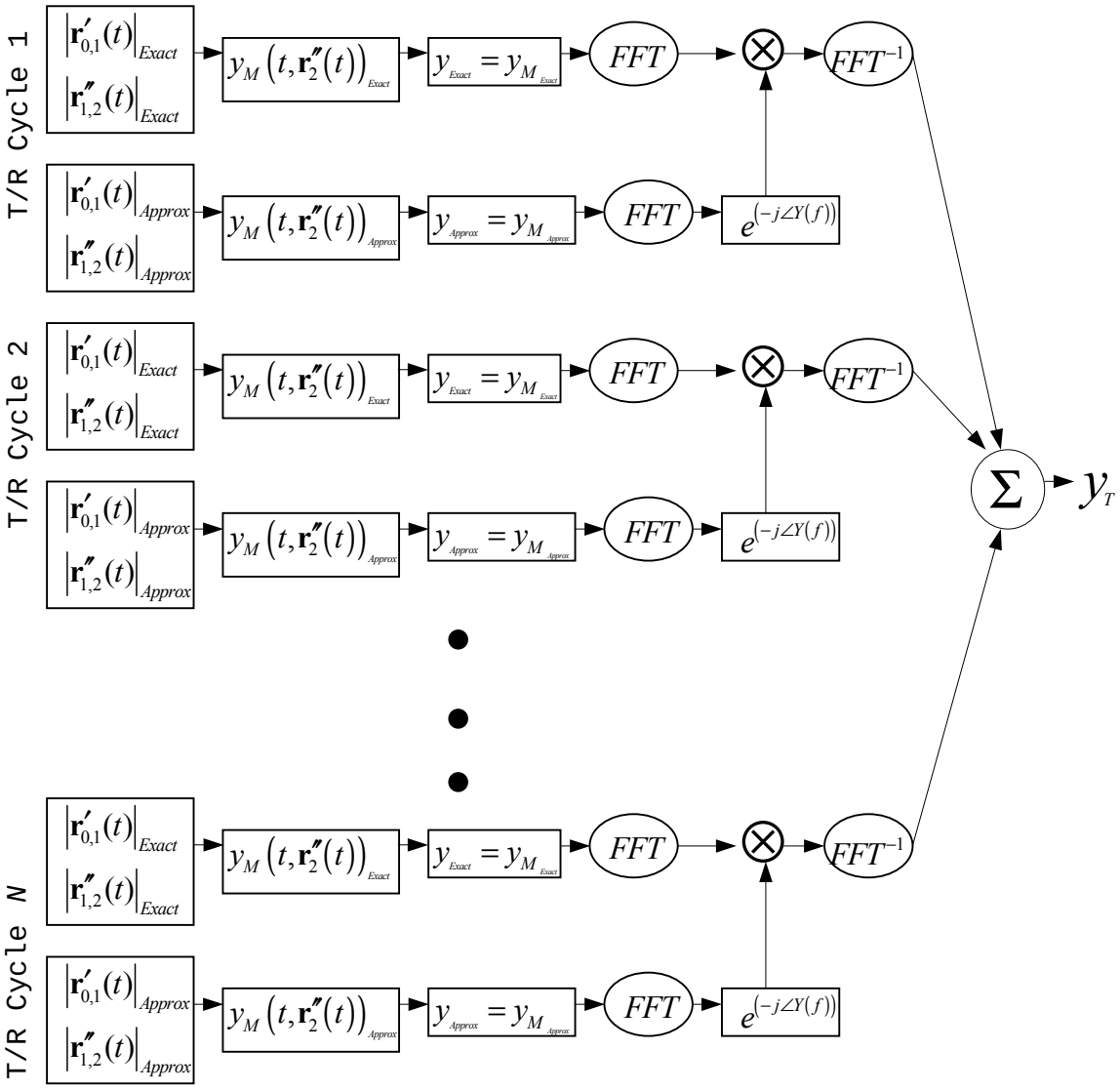

Figure 10. FFT Beamforming Algorithm.

The approximate phase weights are then multiplied by the time-domain Fourier transform of the output electrical

signals determined using the exact method. The exact output electrical signals have now been phase weighted using approximate phase weights. We then compute the inverse Fourier transform of the phase-weighted signals. The resulting time-domain signals are added to produce the total output electrical signal from the SAS array given by

$$y_T(t) = \sum_{n=1}^{N} y_{C_n}\left(t - \left(t_{m_n} + \tau_n\right)\right), \tag{4.10}$$

where N is the total number of transmit/receive cycles used to create the SAS array and $y_{C_n}\left(t - \left(t_{m_n} + \tau_n\right)\right)$ is the output electrical signal from the receiver for the n^{th} transmit/receive cycle after phase weighting. The signals are synchronized in time by subtracting the time delay for each transmit/receive cycle, $\left(t_{m_n} + \tau_n\right)$, where t_{m_n} is the time at the beginning of the n^{th} cycle and τ_n is given by Eq.(3.50). In the FFT beamforming algorithm shown in Fig. 10, we assume that the output electrical signals have been synchronized in time before performing the forward FFT. With the transmit/receive platform constantly in motion, the initial range from the transmitter to the discrete point scatterer and from the scatterer to the receiver will be different at the beginning of each transmit/receive cycle. These initial ranges are updated to reflect the geometry at the beginning of each cycle and, as a result, the propagation delay, τ_n, is recomputed for each transmit/receive cycle. The FFT beamforming procedure is described in detail in [4].

B. PROPAGATION RANGE AND RECEIVED PHASE COMPARISON

1. Stop-and-Hop With Moving Receiver Correction

The performance of the stop-and-hop propagation model is evaluated using Eqs.(4.1) through (4.6) where $\left|\mathbf{r}'_{0,1}(t)\right|_{Exact}$ is given by Eq.(3.49), $\left|\mathbf{r}'_{0,1}(t)\right|_{Approx}$ is given by Eq.(3.24), $\left|\mathbf{r}''_{1,2}(t)\right|_{Exact}$ is given by Eq.(3.48), and $\left|\mathbf{r}''_{1,2}(t)\right|_{Approx}$ is given by Eq.(3.25).

Figure 11 shows the errors introduced by the stop-and-hop approximation for a vehicle speed, V_0, of 2-7 knots, $R = 213$ yards, and frequency, f, of 100 kHz for a single transmit/receive cycle. In this case, the stop-and-hop approximation with the moving receiver correction introduces no error in the estimation of the range from discrete point scatterer to receiver, $\left|\mathbf{r}''_{1,2}(t)\right|$. The error in the estimation of range from transmitter to discrete point scatterer, $\left|\mathbf{r}'_{0,1}(t)\right|$, is, however, significant. The error introduced by the stop-and-hop method results in a maximum percent received phase error of -0.5% at $V_0 = 7$ knots.

At the minimum platform speed of 3 knots, we can investigate estimation errors from the stop-and-hop approximation over all possible target ranges observing the limitations described in Figure 9. Figure 12 shows propagation range and received phase error for $V_0 = 3$ knots, $f = 100$ kHz, with R varied from 25-450 yards. From Figure 12 we can see that the estimation error for $\left|\mathbf{r}'_{0,1}(t)\right|$ and the subsequent phase error increases as the range to the target

decreases. This suggests that the stop-and-hop approximation provides unacceptable performance inside some minimum range.

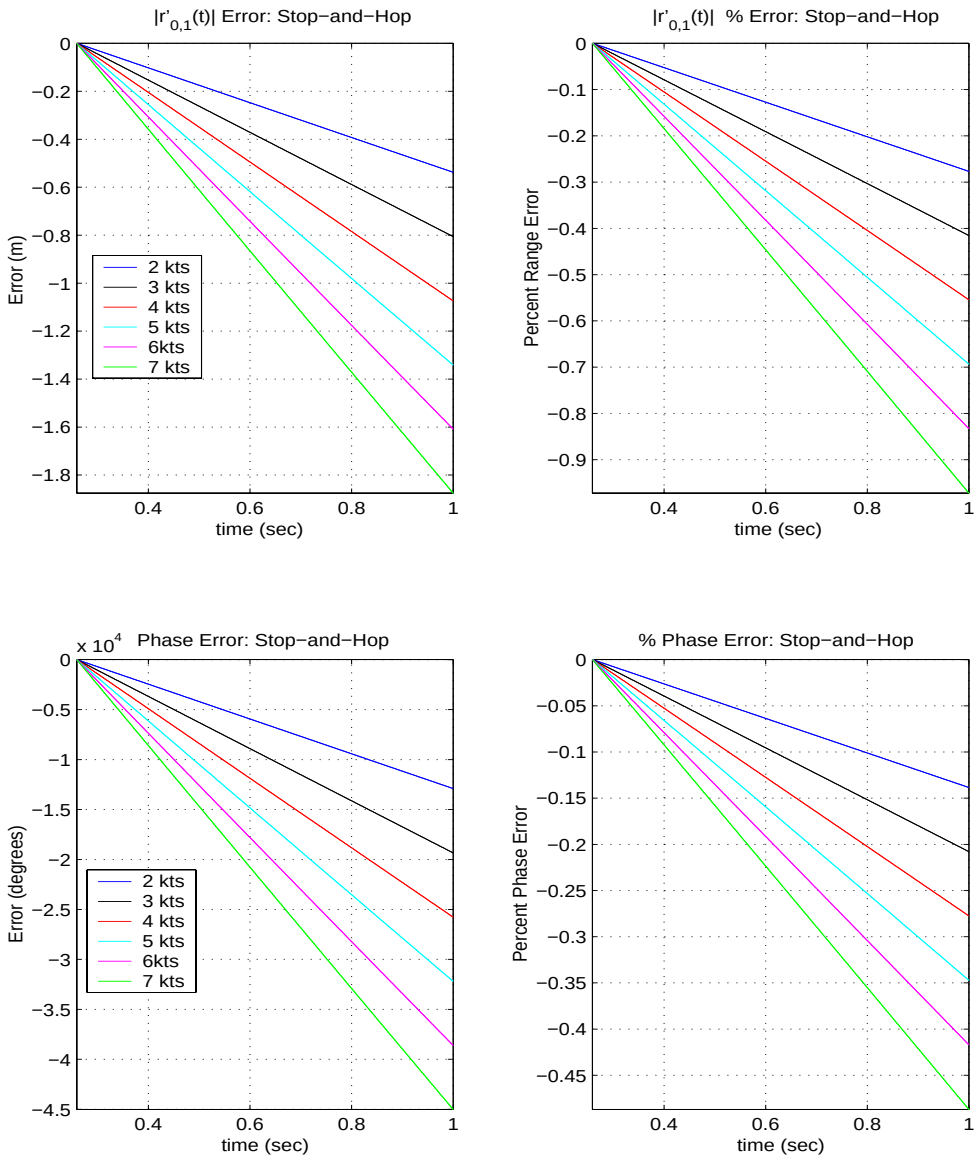

Figure 11. Propagation range and received phase error using the stop-and-hop approximation for $V_0 = 2-7$ knots, $f = 100$ kHz, and $R = 213$ yards.

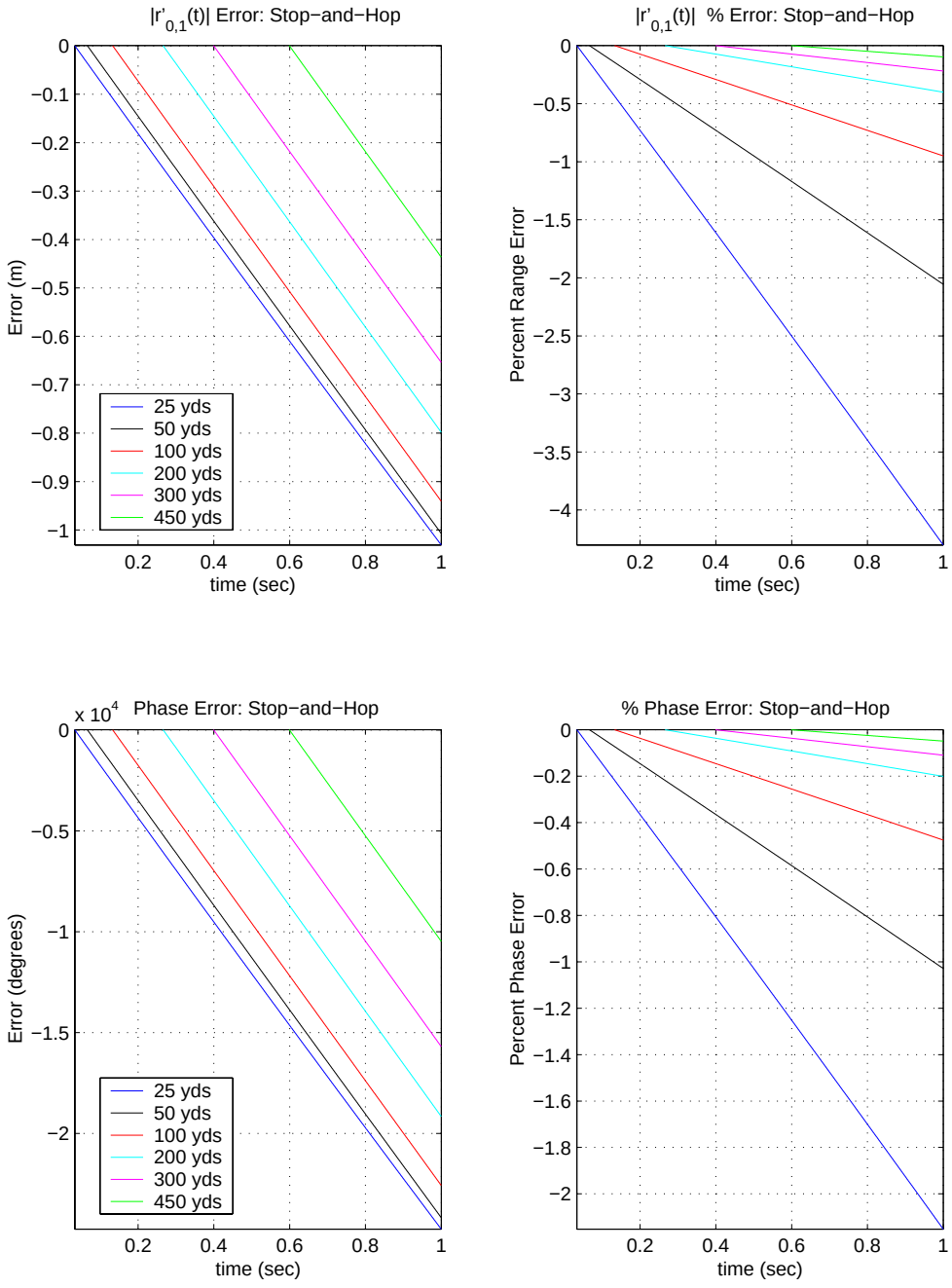

Figure 12. Propagation range and received phase error using the stop-and-hop approximation for $V_0 = 3$ knots, $f = 100$ kHz, and $R = 25 - 450$ yards.

It is interesting to examine the accuracy of the stop-and-hop approximation with the target at different initial angles with respect to the array. The angle ϕ is a cylindrical coordinate measured from array broadside to the target projection in the X-Z plane at the time motion begins, as seen in Figure 8. This simulation is conducted such that R remains constant at 300 yards while ϕ is varied from 0° to 90°. The target depth is set at 150 yards below the platform. The platform speed, V_0, is 5 knots. Figure 13 shows that propagation range and received phase error increase as ϕ increases. This is an important observation since all SAS systems employ the coherent addition of multi-aspect data to form high-resolution images. The ability to accurately image a target at higher aspect angles results in improved along-track image resolution [2].

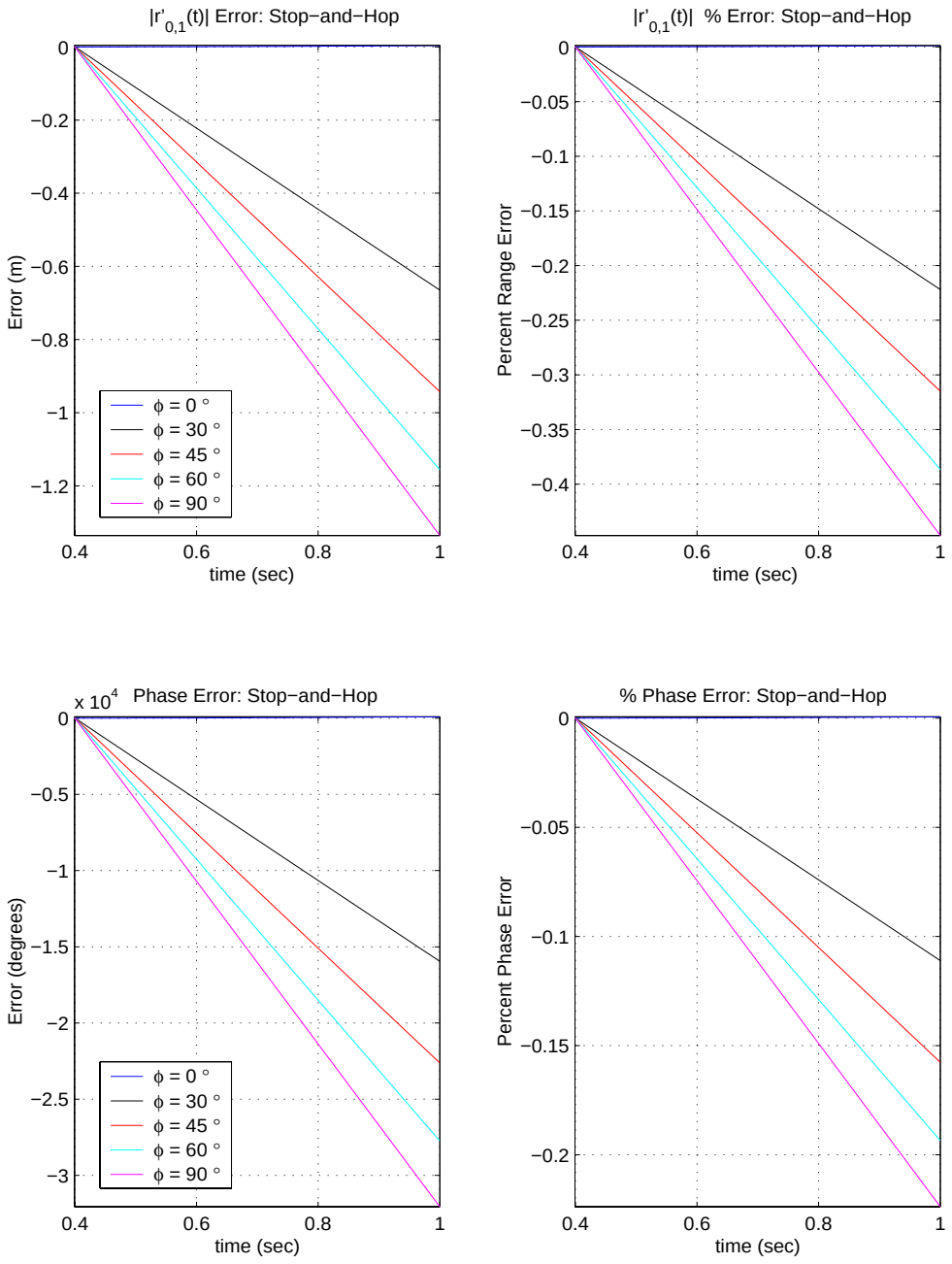

Figure 13. Propagation range and received phase error using the stop-and-hop approximation. Angle ϕ varies from 0° to 90°. Speed $V_0 = 5$ knots, $f = 100$ kHz, and $R = 300$ yards.

2. Binomial Approximation Method

The performance of the binomial approximation method for propagation range estimation is evaluated using Eqs. (4.1) through (4.6) where $\left|\mathbf{r}'_{0,1}(t)\right|_{Exact}$ is given by Eq.(3.49), $\left|\mathbf{r}'_{0,1}(t)\right|_{Approx}$ is given by Eq.(3.32), $\left|\mathbf{r}''_{1,2}(t)\right|_{Exact}$ is given by Eq. (3.48), and $\left|\mathbf{r}''_{1,2}(t)\right|_{Approx}$ is given by Eq.(3.42).

Simulations examining the accuracy of the binomial approximation model were conducted in the same manner as those for the approximate stop-and-hop model. Once again, the binomial approximation estimates of the propagation ranges $\left|\mathbf{r}'_{0,1}(t)\right|$ and $\left|\mathbf{r}''_{1,2}(t)\right|$ and the resulting estimated phase of the acoustic signal incident upon the receiver were compared with the exact solutions for these parameters.

Figure 14 shows the errors introduced by the binomial approximation for a vehicle speed, V_0, of 2-7 knots, $R = 213$ yards, and frequency, f, of 100 kHz for a single transmit/receive cycle. In this case, the binomial approximation introduces extremely small error in the estimation of the range from the transmitter to the discrete point scatterer, $\left|\mathbf{r}'_{0,1}(t)\right|$. Maximum estimation errors for the binomial approximation of $\left|\mathbf{r}'_{0,1}(t)\right|$ are on the order of 10^{-6} meters at $V_0 = 7$ knots. The error from the estimation of range from discrete point scatterer to receiver, $\left|\mathbf{r}''_{1,2}(t)\right|$, is also extremely small. Maximum estimation errors for the binomial approximation of $\left|\mathbf{r}''_{1,2}(t)\right|$ are on the order of 10^{-2}

meters at $V_0 = 7$ knots. The resulting phase error introduced by the binomial approximation method results in a maximum percent received phase error of 0.004% at $V_0 = 7$ knots. Recalling that the stop-and-hop approximation resulted in a maximum percent phase error of -0.5% for the same scenario, it is obvious that the binomial approximation greatly reduces propagation range and received phase estimation error.

At the minimum platform speed of 3 knots, we can again investigate estimation errors from the binomial approximation over all possible target ranges observing the limitations described in Figure 9. Figure 15 shows propagation range and received phase error for $V_0 = 3$ knots and $f = 100$ kHz while R is varied from 25-450 yards. From Figure 15 we can see that the estimation error for $\left|\mathbf{r}'_{0,1}(t)\right|$ increases as the target range, R, increases. Conversely, the range estimation error for $\left|\mathbf{r}''_{1,2}(t)\right|$ decreases as R increases, and is much greater than the range estimation error for $\left|\mathbf{r}'_{0,1}(t)\right|$ in all cases. This results in a phase error that increases as R decreases, a result similar to that observed for the stop-and-hop approximation. This suggests that the binomial approximation also may provide unacceptable performance inside some minimum range. Comparing the stop-and-hop approximation method with the binomial approximation method, we again see that the binomial approximation method introduces much less error in the estimation of propagation ranges and received phase.

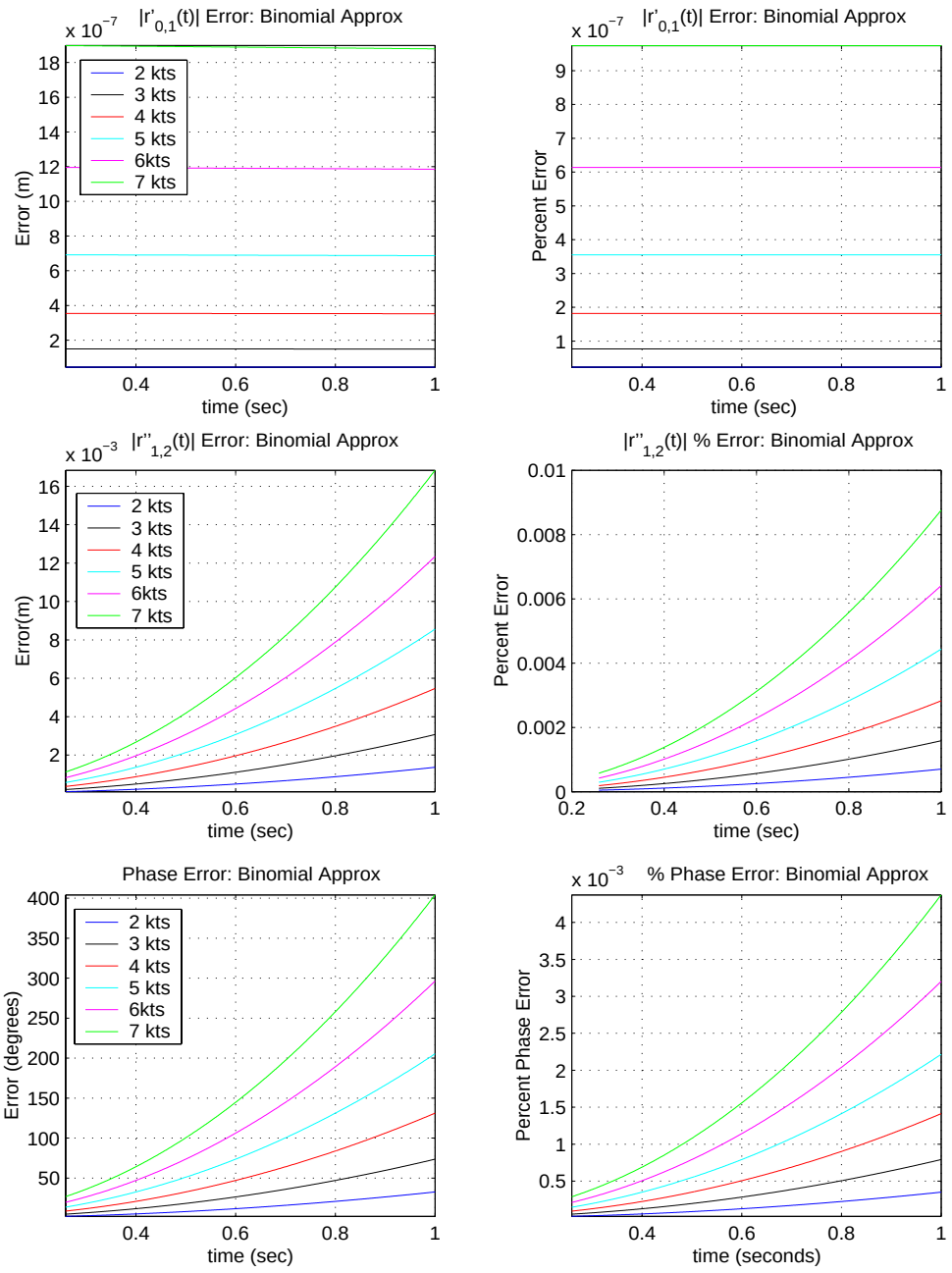

Figure 14. Propagation range and received phase error using the binomial approximation method for $V_0 = 2-7$ knots, $f = 100$ kHz, and $R = 213$ yards.

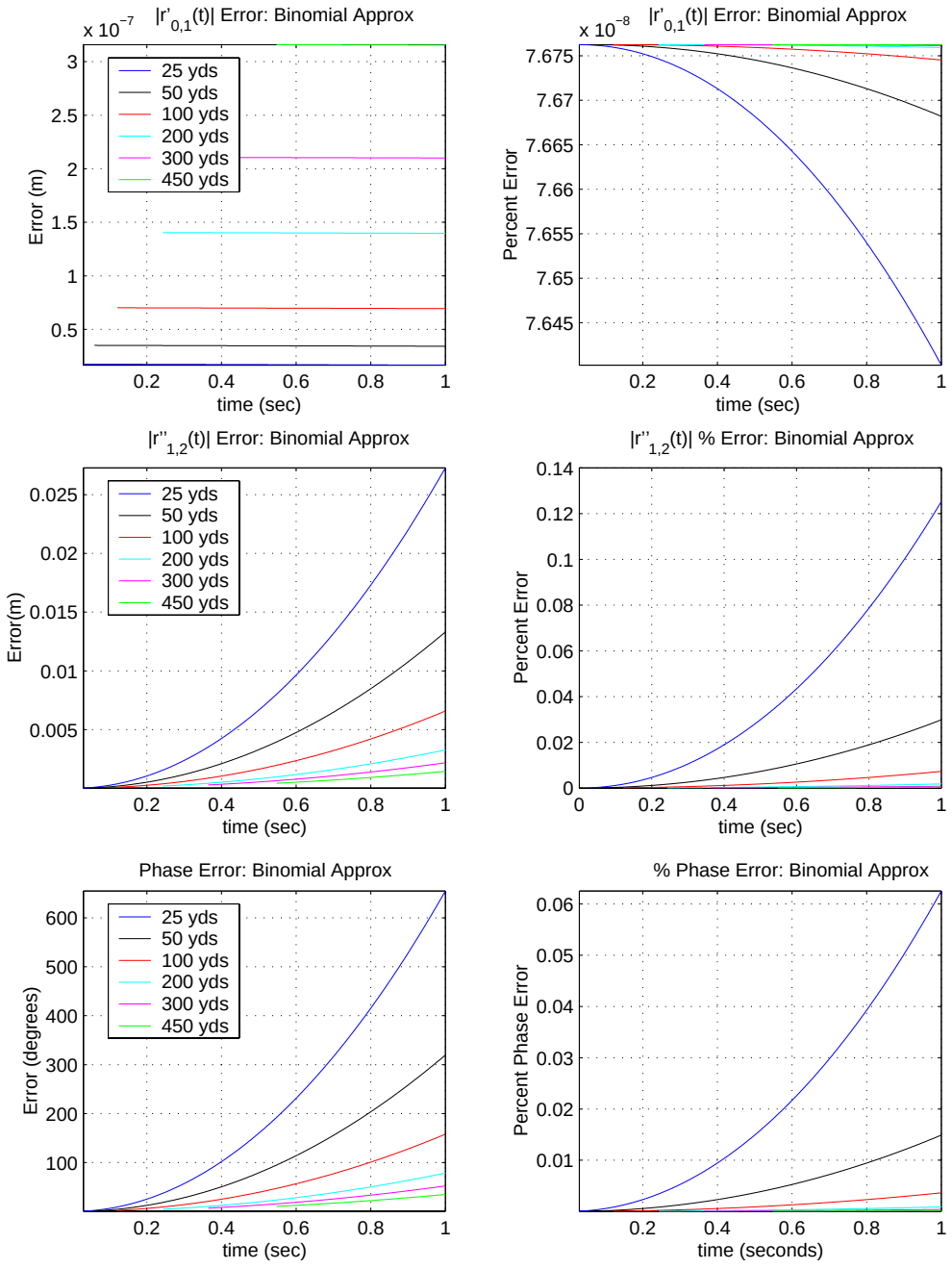

Figure 15. Propagation range and received phase error using the binomial approximation method for $V_0 = 3$ knots, $f = 100$ kHz, and $R = 25 - 450$ yards.

We can also examine the accuracy of the binomial approximation method with the target at different initial angles with respect to the array. The angle ϕ is a cylindrical coordinate measured from array broadside to the target projection in the X-Z plane, as seen in Figure 8. This simulation is conducted such that R remains constant at 300 yards while ϕ is varied from 0° to 90°. The target depth is set at 150 yards below the platform. The platform speed, $V_0 = 5$ knots. Figure 16 shows that propagation range and received phase error decrease as ϕ increases. This suggests that the binomial approximation method would be able to more accurately combine the multi-aspect data inherent to SAS systems. Once again, we can see that the binomial approximation introduces a maximum of 0.002% phase error compared to -0.25% phase estimation error per transmit/receive cycle introduced by the stop-and-hop approximation.

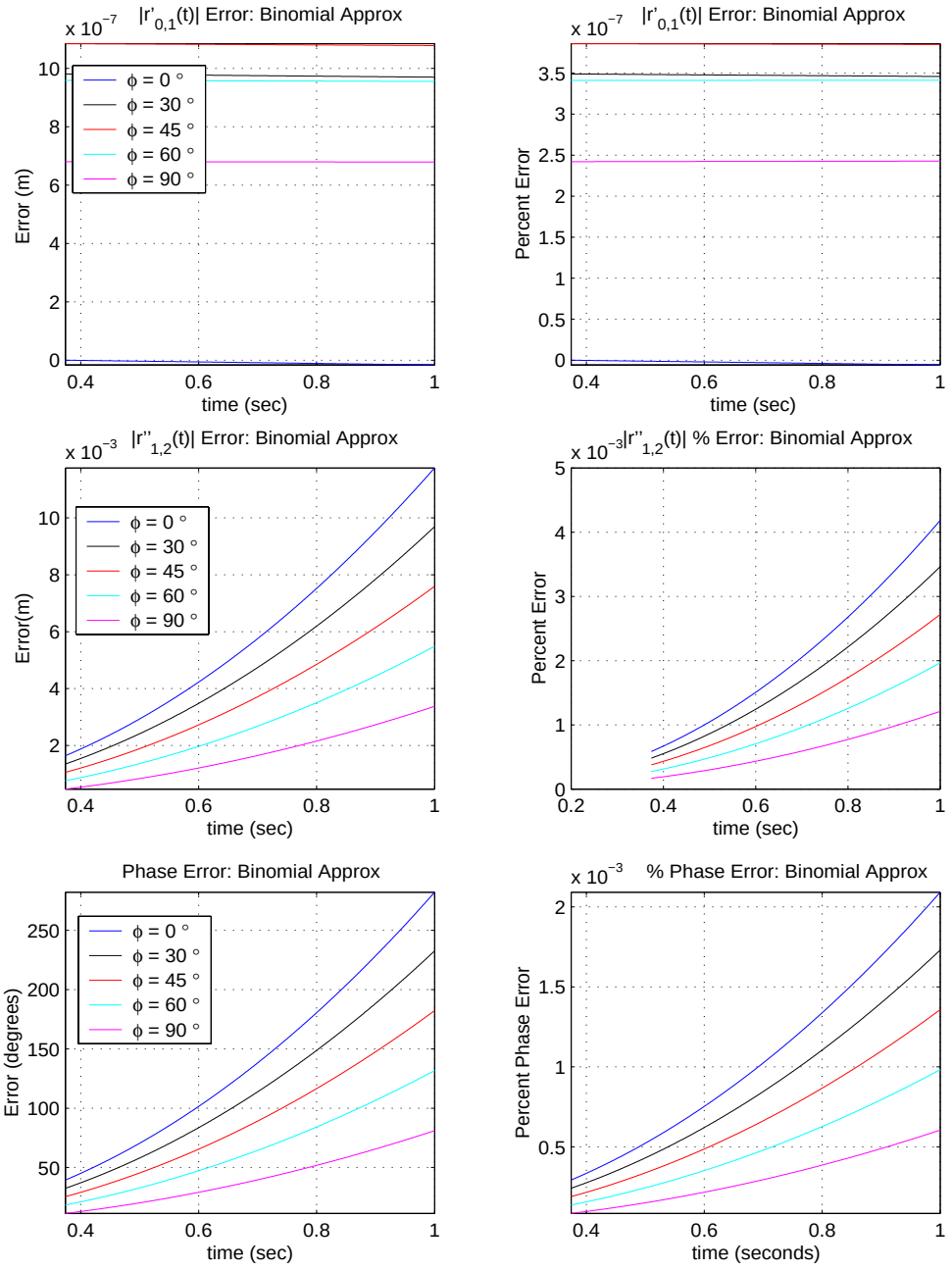

Figure 16. Propagation range and received phase error using the binomial approximation. Angle ϕ varies from 0° to 90°. Speed $V_0 = 5$ knots, $f = 100$ kHz, and $R = 300$ yards.

C. FFT BEAMFORMING SIMULATIONS

To provide some insight into the performance of the various propagation models when applied to a SAS system, each model was used to calculate the phase weights for use in an FFT beamforming algorithm as described in IV.A.3, where $f_1 = 10$ kHz, $f_2 = 20$ kHz, and $f_3 = 30$ kHz.

The array is synthesized as the vehicle travels at the designated speed in a straight line along the positive Z axis.

Figure 17 shows results of FFT beamforming with (a) $V_0 = 3$ knots and (b) $V_0 = 7$ knots. The array is synthesized using 10 transmit/receive cycles with the target at an initial range, R, of 213 yards and $\phi = 45^\circ$. Phase weighting the output electrical signals using the binomial approximation method to determine received phase of the incident acoustic signal at both 3 and 7 knots produces a waveform that is almost exact. The errors in the stop-and-hop approximation, however, are significant and phase weighting the output electrical signals using this method results in very low array gain. The poor performance of the stop-and-hop approximation results from the relatively high error in the received acoustic signal phase estimate.

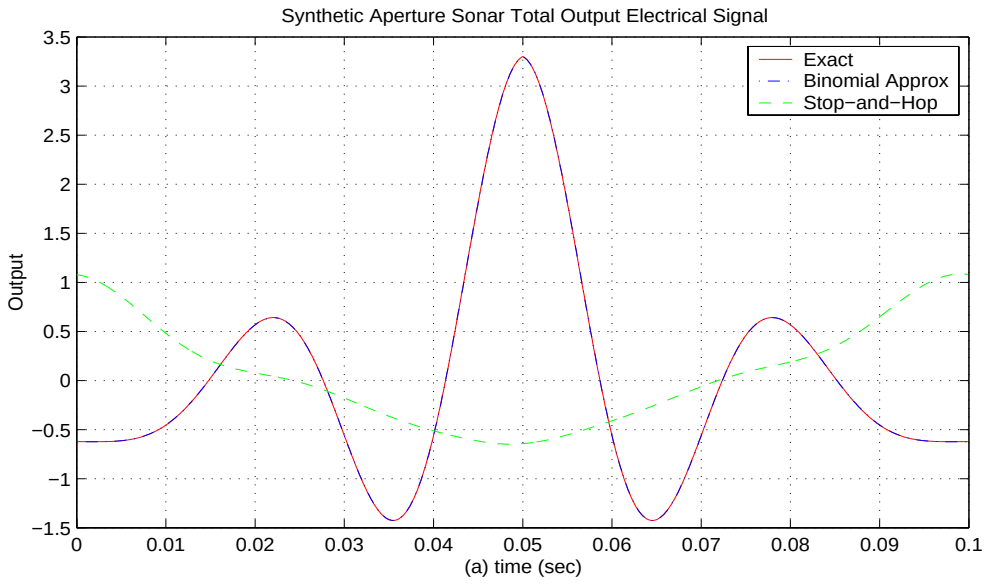

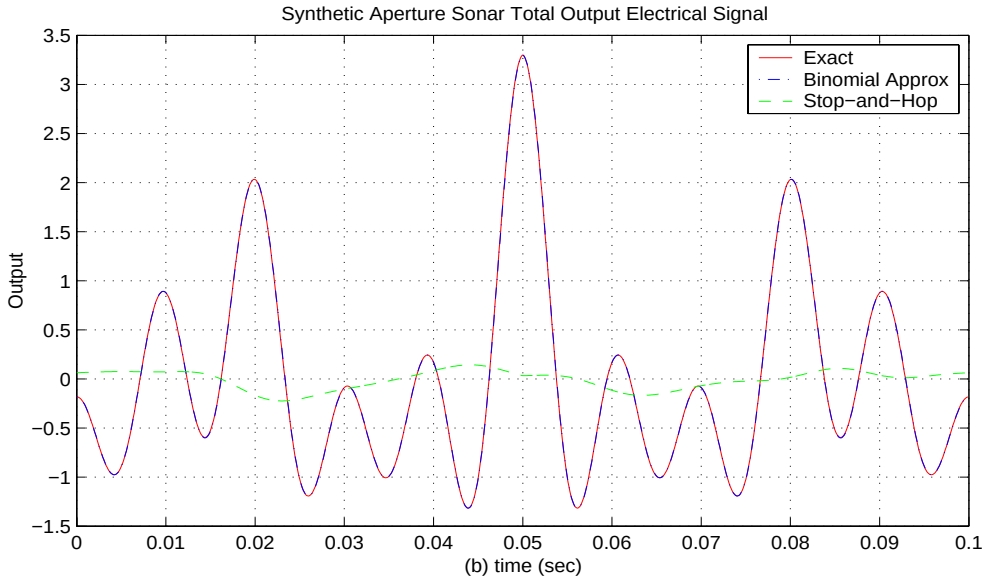

Figure 17. FFT beamforming with (a) $V_0 = 3$ knots and (b) $V_0 = 7$ knots. The array is synthesized using 10 transmit/ receive cycles with the target at an initial range, R, of 213 yards and $\phi = 45^\circ$.

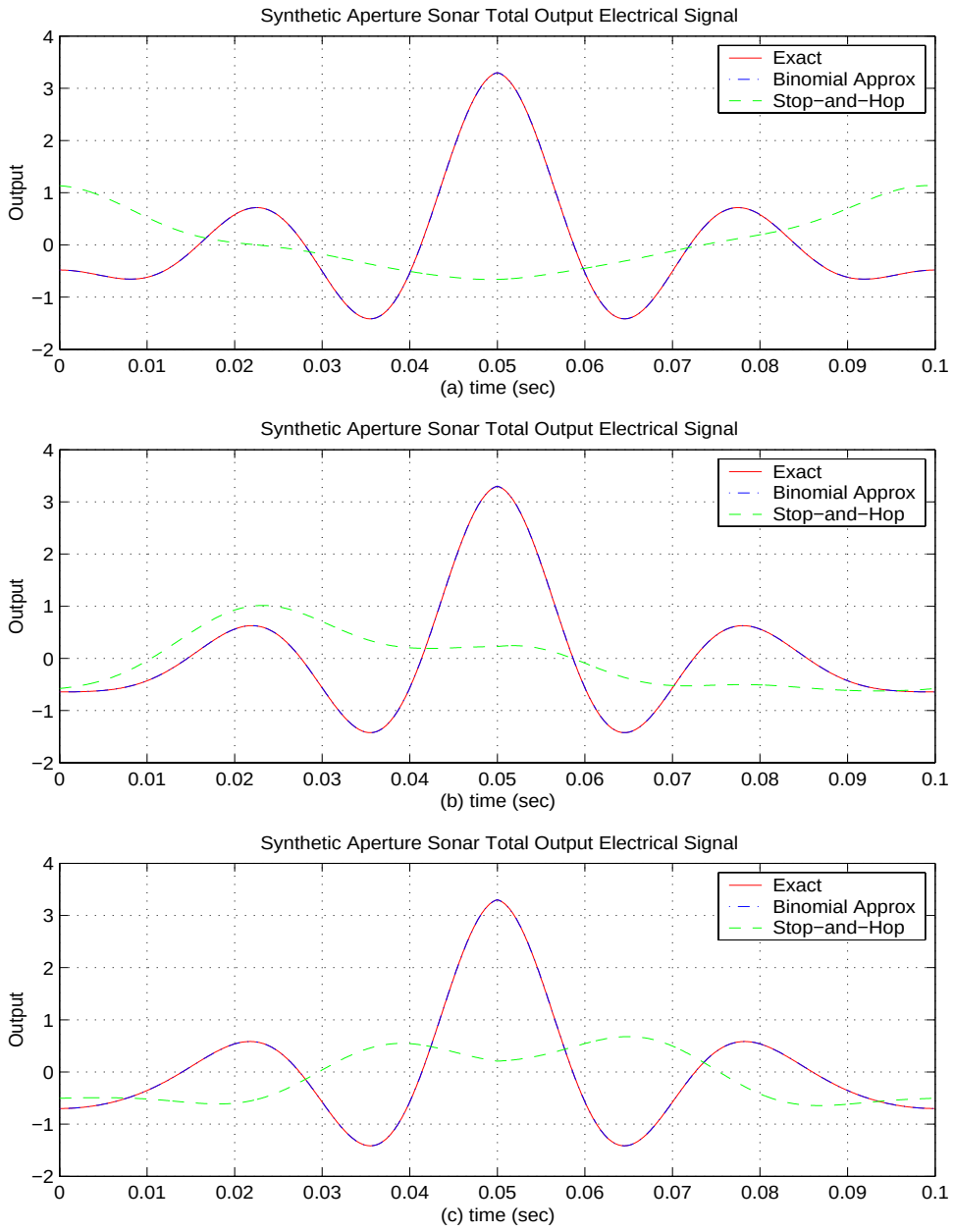

Figure 18. FFT beamforming with $V_0 = 3$ knots and (a) $R = 100$ yards, (b) $R = 250$ yards, and (c) $R = 500$ yards. The initial target angle, $\phi = 45^\circ$. The array is synthesized using 10 transmit/receive cycles.

Figure 18 shows the results of FFT beamforming with $V_0 = 3$ knots and (a) $R = 100$ yards, (b) $R = 250$ yards, and (c) $R = 500$ yards. The initial target angle, $\phi = 45^\circ$ in all three cases and the array is synthesized using 10 transmit/receive cycles. We again see that phase weighting the output electrical signals using the binomial approximation of received acoustic signal phase is almost exact. Phase weighting using the stop-and-hop approximation method for estimating received acoustic signal phase results in very low array gain in all cases.

The errors introduced by the binomial approximation method seen in Figures 14, 15, and 16 are not large enough to significantly affect the steering and focusing of the beam pattern for typical vehicle speeds and target ranges. When the array is placed within 1 yard of the target and the vehicle is allowed to travel at 7 knots, however, the binomial approximation errors become evident. Figure 19 shows the results of FFT beamforming with $R = 1$ yard, $V_0 = 7$ knots, and $\phi = 45^\circ$ for an array synthesized with 10 transmit/receive cycles. In this case, the errors introduced in the estimation of propagation ranges with the binomial approximation method are a significant percentage of the total range.

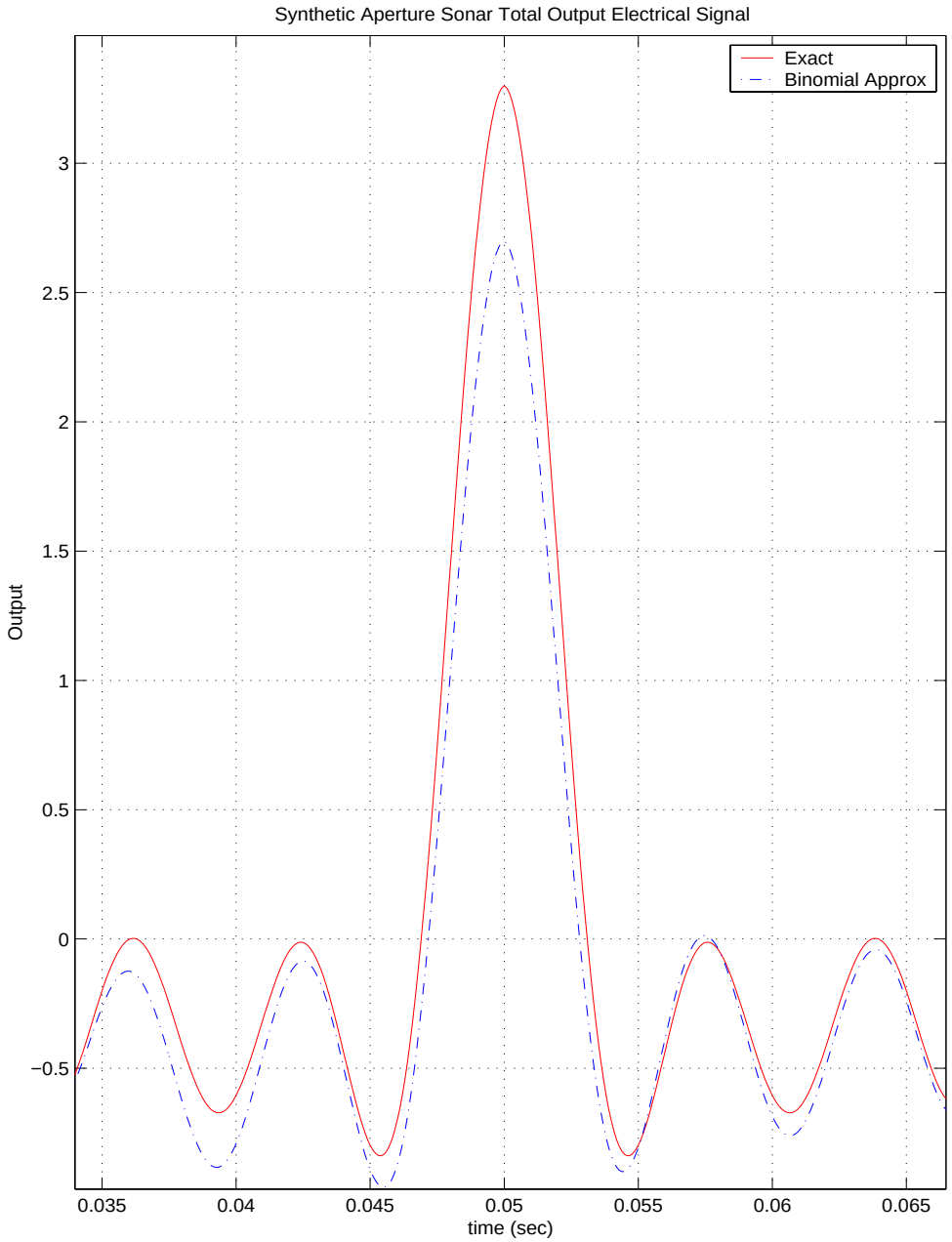

Figure 19. FFT beamforming with $R = 1$ yard, $V_0 = 7$ knots, and $\phi = 45^\circ$ for an array synthesized with 10 transmit/ receive cycles.

D. SUMMARY

The propagation ranges and received acoustic signal phase can be estimated using both the stop-and-hop method and the binomial approximation method. Both methods introduce some error into the calculation of propagation ranges and received acoustic signal phase. Simulation results indicate that the error introduced by the binomial approximation is significantly lower than the error introduced by the stop-and-hop approximation for typical LMRS vehicle speeds and target ranges. Estimates of received phase from both the stop-and-hop approximation and the binomial approximation methods were used to phase weight the output electrical signals in an FFT beamforming algorithm. The errors introduced by the stop-and-hop approximation method significantly degrade the performance of the FFT beamforming algorithm. Conversely, the binomial approximation method for received acoustic signal phase estimation can be used to accurately phase weight the output electrical signals at typical LMRS vehicle speeds and target ranges. The thesis conclusions are presented in the next chapter.

THIS PAGE INTENTIONALLY LEFT BLANK

V. SUMMARY AND CONCLUSIONS

This chapter provides a summary of the propagation range and received acoustic signal phase estimation methods. Based on the simulations presented in the last chapter, the accuracy of the stop-and-hop approximation and the binomial approximation methods is analyzed. Finally, further research in SAS acoustic signal processing is recommended.

A. SUMMARY

Accurate estimation of acoustic signal propagation range and received phase is critical to SAS system performance. To determine the phase of the acoustic signal incident upon the receiver at all locations along the synthetic array, the time-varying range from the transmitter to the target and from the target to the receiver must be determined. The estimated phase of the received acoustic signal can then be used to steer and focus the beam pattern of the synthetic aperture array.

The SAS concept is currently being applied to the problem of water-borne mine classification and imaging in the Navy's Long-Term Mine Reconnaissance System (LMRS). This requires high resolution imaging at long ranges. Under these conditions, small errors in the estimates for propagation range and subsequent phase estimates can significantly degrade the SAS system's ability to steer and focus the array beam pattern.

This thesis analyzed the performance of the stop-and-hop approximation and the binomial approximation models for

determining propagation range and received phase of acoustic signals for a SAS system imaging a stationary target. The stop-and-hop method, presented in [6], initially assumes that the vehicle is stationary during transmission, propagation, and reception of the acoustic signal. A simple correction is applied to account for receiver motion. The binomial approximation method, presented in [5], develops equations for the range from transmitter to target and from target to receiver for the general problem of bistatic scattering. Approximate solutions for propagation range equations are obtained by performing a binomial expansion of the propagation range equations. The derivations of this technique place some restrictions on the simulation parameters, but at the same time ensure minimal estimation error.

The stop-and-hop approximation method and the binomial approximation method were compared using simulations that exactly determine the acoustic signal propagation range and received phase for a SAS system imaging a stationary target. This exact method, presented in [9], for the first time allows us to investigate the accuracy of common approximations and their effect on SAS system performance.

This thesis also presented an overview of the model used to simulate the propagation of acoustic signals for a SAS system. In the simulations presented, the ocean is treated as a linear, time-variant, space-variant filter. The complex frequency response of the ocean filter is the primary focus of the simulations presented.

B. CONCLUSIONS

Simulations presented in this thesis are based on typical LMRS vehicle speeds and target ranges. Performance of the different approximation methods was compared for a single transmit/receive cycle and then the estimates of received acoustic signal phase were used to compare the performance of each method applied to an FFT beamforming algorithm.

The stop-and-hop approximation introduced a maximum of -0.5% received phase error with the vehicle traveling at the LMRS maximum specified speed and at the maximum target range. The error in propagation range and received phase estimation increased as target range increased, resulting in a maximum of -2.5% received phase estimation error with the transmit/receive platform at the minimum LMRS speed and the target at 25 yards. The estimation errors introduced by the stop-and-hop approximation method are small, but significant. This is best demonstrated when the stop-and-hop approximation method is used to determine the phase weights in an FFT beamforming algorithm applied to a SAS array. The error introduced by the stop-and-hop approximation method significantly degraded the performance of the FFT beamforming algorithm. It was also evident that the accuracy of the stop-and-hop approximation method decreased as the target aspect angle increased. This suggests that the stop-and-hop approximation method is poorly suited to modern SAS techniques that combine multi-aspect data to improve image resolution.

The binomial approximation method estimated acoustic signal propagation range and received phase per trans-

mit/receive cycle with much less error than the stop-and-hop approximation method. At the maximum LMRS speed and target range, the received phase estimation error was approximately 100 times less than the error introduced by the stop-and-hop approximation. Similarly, at low platform speeds and close target ranges the estimation error introduced by the binomial approximation method was 1000 times less than the error introduced by the stop-and-hop method. In fact, the errors introduced by the binomial approximation were insignificant when the estimates of received acoustic signal phase were used to phase weight the output electrical signals of the array in an FFT beamforming algorithm. Only at very close target ranges (less than 1 yard) and high platform speeds did the errors introduced by the binomial approximation significantly affect the performance of the SAS system. In contrast to the stop-and-hop approximation method, the accuracy of the binomial approximation method improved as the target aspect angle increased.

The propagation range and received acoustic signal phase can be determined exactly for the SAS system using the techniques presented in [9]. These exact solutions do not add significant complexity to the SAS signal-processing problem while eliminating errors introduced by approximate methods. These exact solutions place no restrictions on target range and vehicle velocity, allowing for maximum flexibility as SAS systems evolve.

C. RECOMMENDATIONS FOR FUTURE RESEARCH

This thesis considered improvements to SAS system beamforming using the exact and binomial approximation methods for determining propagation range and received acoustic signal phase versus using the stop-and-hop approximation. The methods presented in [9] also provide exact solutions for the time-varying angles of incidence and scatter at the discrete point scatterer and the time-varying angles of incidence at the receiver. This additional information should be incorporated into models of the scattering functions for mines and mine-like objects since scattering functions are not only functions of frequency, but also functions of the angles of incidence and scatter. Scattering functions should be included in future simulations in order to determine their impact on SAS system performance. Using LMRS operational parameters, typical oceanographic data, and real world target simulations, and end-to-end SAS simulation should be developed. The simulations would be critical to the development of SAS operational guidelines, capabilities, and future improvement.

THIS PAGE INTENTIONALLY LEFT BLANK

LIST OF REFERENCES

1. H. D. Griffiths, "Radar and sonar imaging – A tutorial introduction," *Recent Developments in Radar and Sonar Imaging Systems: What's Next?,* pp. 1/1-1/7, IEE, London, December 1995.

2. M. Medeiros, *AN/BLQ-11 (LMRS) Detection and Classification Sonar System Overview,* NUWCDIVNPT Brief, Newport, Rhode Island, 17 May 2001.

3. P. T. Gough and D. W. Hawkins, "A short history of synthetic aperture sonar," *Proceedings of the Geoscience and Remote Sensing Symposium*, Vol. 2, pp. 618-620, IEEE Press, New York, July 2001.

4. L. J. Ziomek, *Fundamentals of Acoustic Field Theory and Space-Time Signal Processing*, CRC Press, Boca Raton, Florida, 1995.

5. L. J. Ziomek, "Pulse propagation and bistatic scattering," Technical Report No. NPS-EC-02-001, Naval Postgraduate School, Monterey, California, October 2001.

6. W. W. Bonifant Jr., "Interferometric synthetic aperture sonar processing," MSEE Thesis, Georgia Institute of Technology, Atlanta, Georgia, July 1999.

7. S. L. Jordan, "If we go to war," Corpus Christi Caller-Times, December 22, 2002, [www.caller.com/ccct/local_news/article/0,1641,CCCT_811_1626769,00.html], January 15,2003.

8. Boeing integrated defense systems, http://www.boeing.com/defense-space/infoelect/lmrs/sld005.htm, September 2002.

9. L. J. Ziomek, "The modeling of bistatic scattering with moving platforms," Technical Report No. NPS-EC-03-001, Naval Postgraduate School, Monterey, California, October 2002.

THIS PAGE INTENTIONALLY LEFT BLANK

INITIAL DISTRIBUTION LIST

1. Defense Technical Information Center
   Ft. Belvoir, VA

2. Dudley Knox Library
   Naval Postgraduate School
   Monterey, CA

3. Dr. Lawrence J. Ziomek
   Naval Postgraduate School
   Monterey, CA

4. Dr. Xiaoping Yun
   Naval Postgraduate School
   Monterey, CA

5. Michael R. Medeiros
   Naval Undersea Warfare Center
   Newport, RI